

TOPICAL REVIEW

Atomically crafted spin lattices as model systems for quantum magnetism

A Spinelli, M P Rebergen and A F Otte

Department of Quantum Nanoscience, Kavli Institute of Nanoscience
Delft University of Technology, Lorentzweg 1, 2628 CJ Delft, The Netherlands

E-mail: a.f.otte@tudelft.nl

Abstract. Low-dimensional quantum magnetism presents a seemingly unlimited source of rich, intriguing physics. Yet, as realistic experimental representations are hard to come by, the field remains predominantly theoretical. In recent years, artificial spin structures built through manipulation of magnetic atoms in a scanning tunnelling microscope have developed into a promising testing ground for experimental verification of theoretical models. Here we present an overview of available tools and discuss recent achievements as well as future avenues. Moreover, we show new observations on magnetic switching in a bistable bit that can be used to extrapolate information on the magnetisation of the microscope tip.

Contents

1	Introduction	2
2	Motivation: low dimensional quantum magnetism	2
3	Measurement techniques	5
3.1	Atom manipulation	5
3.2	Inelastic electron tunnelling spectroscopy	7
3.3	Functionalized spin-polarized tips	10
4	Modelling the environment	12
4.1	Magnetic anisotropy	12
4.1.1	Strain induced variation of magnetic anisotropy	15
4.2	Heisenberg interaction	17
4.3	Kondo screening	18
5	Magnetic bistability	19
5.1	Telegraph noise detection	21
5.2	Spin wave mediated reversal	23
5.3	Back-action onto the tip	24
6	Conclusions and outlook	29

1. Introduction

Magnetism is a collective phenomenon. Whereas a single spin is known to behave perfectly quantum mechanically, classical magnetic stability sets in only when many spins are coupled together. In between these two regimes there is a size domain – anywhere between two and, say, hundreds of spins – in which the system is large enough to speak of collective spin excitations, but still small enough in order for these excitations to be coherent throughout the system. It is in this region that we can learn how the collective quantum mechanical behaviour of interacting spins eventually gives rise to the emergence of the magnetic properties found in materials on the macroscopic scale.

Atomic assembly of magnetic structures through low temperature scanning tunnelling microscopy (STM) poses an intriguing method for entering this size domain. Less than 25 years after the first demonstration of atom manipulation [1], we have now come to a time where it is possible not only to detect a single atom’s magnetization [2, 3], but also to analyse and control its magnetocrystalline anisotropy [4, 5, 6, 7], measure its Kondo coupling to the substrate electrons [8, 9, 10, 11], tune and read-out interatomic exchange coupling between two neighbouring atoms [12, 13, 14] and build extended atomic spin chains and structures [15, 16, 17]. Even the first steps towards technological usage of these abilities are taken in the form of an atomic scale logic gate [18] and of atom-based bits showing extended magnetic lifetimes [19, 20, 21, 22]. We believe that these techniques can be equally valuable for the more fundamental challenge of exploring quantum magnetism.

In this review we will focus on experiments performed on magnetic atoms deposited on thin insulating layers, specifically Cu_2N on $\text{Cu}(100)$. This surface provides significant decoupling between the atoms and the bulk electrons in the metal below, resulting in relatively long lived spin states. The magnetic atoms we will focus on are $3d$ -metals, in particular Fe and Co. Fe on Cu_2N has a spin $S = 2$ and its ground state lies in the subspace with highest spin projection ($m = \pm 2$). On the other hand, Co has spin $S = 3/2$ and the ground state is in the multiplet with smallest spin projection ($m = \pm 1/2$). As we will see in the next sections, those two magnetic atoms have very different properties, not only due to the difference between integer and half-integer spins. On this surface, they develop a different magnetocrystalline anisotropy, that gives rise to dissimilar behaviours both for a single atom and for structures composed of few atoms. Moreover, Co turns out to be Kondo-screened while Fe is not. In addition to reviewing existing work we will present novel results on the back-action of the atomic spin structures onto the magnetic state of the functionalized spin-polarized tip that is used to probe them.

2. Motivation: low dimensional quantum magnetism

Inside a magnetically ordered material, all the atomic moments point in a specific direction: once the magnetization direction of one atom is fixed, the n th atom’s

magnetization will have a specific orientation, determined by the exchange interaction between neighbouring atoms. However, since the macroscopic magnetic state results from the interactions between all the constituent atomic spins, the emergence of magnetic order is very difficult to predict. In some materials magnetic order does not set in at all, regardless of system size. An interesting approach to gain insight into these processes is to study interactions on the scale of individual spins in a finite system, while slowly increasing the number of participating spins.

The two best known ordered materials are ferromagnets (FM) and antiferromagnets (AFM). In a ferromagnet, the lowest energy state is one where all spins are parallel to each other, giving rise to a net magnetization that is preserved even when the external magnetic field $\mathbf{B} = 0$. In an antiferromagnetic material, in the ground state the spins exhibit antiparallel alignment, which gives rise to a zero net magnetization even though the magnetic order is present.

In one dimension, the collective excitations from the ground state have a different nature for FM and AFM spin structures, as depicted in figure 1. In a ferromagnetic phase, the excited states have the form of *magnons*: single spin flipped by $\Delta m = 1$ surrounded by two bound domain walls (figure 1a). These domain walls are delocalised inside the structure and always propagate in pairs. The classical analogous of a magnon can be visualized as a spin wave, a coherent precession of the local spin expectation value around the common magnetization direction [23]. In an antiferromagnet, the elementary excitations are *spinons*. In this case the single flipped spin is surrounded by two domain walls that are not bound and can propagate independently. Each spinon carries a net spin value of $1/2$ (figure 1b). These fractional quasiparticles are easier to visualize in the Ising limit [24, 25], in which all the spins exist only in two possible orientations. In this case, a spinon is simply a domain wall between two different antiferromagnetic phases. In the more complex Heisenberg case (which will be discussed in section 4.2) a single spin flip needs to be visualized with more pairs of spinons [23].

When considering quantum spins, we may enter some regimes in which things can get more complex and the system can host exotic excitations and lose long range order. In particular, the system can become a quantum spin liquid (QSL), a spin system that is supposed to hold many exotic properties and has attracted massive theoretical interest after its first proposal, made by Anderson in 1973 [26]. A QSL is a collective spin state whose magnetic order is suppressed due to quantum fluctuations, leading to liquid-like properties among the spins, and it can emerge in presence of frustration or in low dimensions [27, 28].

The type of ground state and the nature of the excitations of a coupled spin system strongly depend on several parameters [29]: the magnitude of the spin, the interaction strength (we already mentioned the profound differences between FM and AFM coupling and the importance of long range order for the emergence of classical stability) and the geometry of the system. The magnitude of the spin is what makes it quantum: the case $S \rightarrow \infty$ corresponds to the classical limit, while $S = 1/2$ is the extreme quantum limit. Also integer and half-integer spins are predicted to show quite different behaviours.

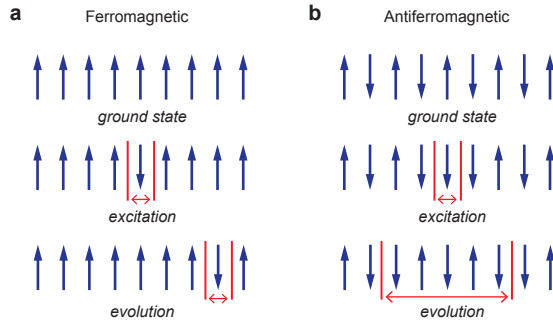


Figure 1. (a) Magnon excitation and its evolution inside a ferromagnetic chain. In the ground state all the spins are in parallel alignment within each other. A magnon can be represented as a single reversed spin surrounded by two domain walls. It can propagate along the chain, but the domain walls will stay bounded to each other. (b) Same as (a) but for an antiferromagnetic chain, in the Ising limit. In the ground state, the spins are in antiparallel alignment. An excitation is achieved by creating two domain walls that separate two different AFM phases. Those two fractional excitations can independently propagate along the chain.

For instance, while an antiferromagnetic chain composed of half integer spins has a relatively long range ordered ground state, the same chain composed of integer spins is predicted to lose this order even at zero temperature (the Haldane model [30]). The dimensionality of the system plays a critical role: in one- and two-dimensions there is no long range magnetic order, as stated in the Mermin–Wagner theorem[31]. Finally, quantum fluctuations in a spin system can be enhanced in presence of frustration, which implies a conflict in minimizing the coupling energies associated with different spin pairs; these conflicts arise mainly because of the lattice topology or due to the presence of competing further-neighbour interactions [32].

The literature on quantum magnetism in general and on quantum spin liquids in particular is quite extensive; for a review see for instance Refs. [33] and [34]. Yet, despite the large interest in this topic from a theoretical viewpoint, the possibilities for experimental verification remain limited. On the one hand, magnetic materials are studied from the top down, using spatially averaging techniques such as neutron diffraction [23]. While offering highly detailed information in reciprocal space, these techniques lack the possibility to probe materials locally or as function of system size. A different approach is provided by the community of ultracold atoms, where optical lattices containing spins are built from the bottom up [35]. The opportunity to create spin lattices with atomic precision in a real condensed matter environment, as described in this review, offers a large range of new possibilities that complement those offered by existing methods.

3. Measurement techniques

The scanning tunnelling microscope (STM) was invented in 1981 by Rohrer and Binnig [36, 37] as a tool that, by using vacuum tunnelling in a controlled way, was able to image conductive surfaces with unprecedented atomic resolution. Even though the STM is most famous for its imaging capabilities, this instrument can also be used for various techniques needed for surface characterization. In particular, single atoms and molecules can be manipulated and their local electronic and magnetic properties can be investigated via inelastic electron tunnelling spectroscopy (IETS). In this section we will describe how atom manipulation and tunnelling spectroscopy work, specifically in the case of magnetic atoms on Cu_2N , and give insight into the possible models to reproduce measured spectra. Also, we will discuss spin-polarized measurements and how the magnetic state of an atom can be probed with a magnetic STM tip.

3.1. Atom manipulation

The most common form of atom manipulation is lateral manipulation, where atoms are dragged along a flat metal surface. This is possible due to the relatively weak van der Waals binding of the atoms to the surface: when the metal tip is lowered towards the atom, due to the additional van der Waals attraction of the tip the atom may fall into the combined potential well of both tip and surface, the minimum of which is located above the atom’s original position. Combinations of materials that are often used for this technique are Fe atoms on Cu(111) (which is known for the quantum corral [38] and the atomic OR gate [18]), CO molecules on Cu(111) (in the molecule cascades [39] and ‘molecular graphene’ [40]), and Fe atoms on Pt(111) [6]. The {111} crystal orientation is particularly suitable for lateral atom manipulation due to its dense packing.

Lateral manipulation does not work on the $\text{Cu}(100)\text{-}c(2 \times 2)\text{N}$ surface [41], hence referred to as Cu_2N , the two-dimensional lattice which is shown in figure 2a. According to density functional theory (DFT) calculations, the covalent Cu–N bonds form a fishnet-shaped two-dimensional network on the surface [4]. As confirmed by STM topography, Fe atoms, upon being evaporated onto the cold surface, bind on the Cu sites of this lattice. Here they replace the position inside the covalent network previously held by the underlying Cu atom such that the resulting local structure can be seen as a N–Fe–N molecule. The same behaviour as for Fe was found for Mn and Co atoms [15, 11].

Since 3d-metals tend to be strongly bound to the Cu_2N surface, a different technique is needed to move atoms, commonly called vertical manipulation [42, 15]. This technique is based on the actual transfer of the atom from the surface to the tip, and then again to the surface, allowing for an atomic precision drop-off. When the tip is few ångströms away from the surface, at a common imaging distance, the system can be seen as an asymmetric double potential well: the atom has two possible stable positions, one on the surface and one on the tip, that are separated by an energy barrier (figure 2b), with global minimum on the surface side. By letting the tip closer to the atom, and applying a negative voltage to the tip, the potential well gets distorted favouring the tip side of

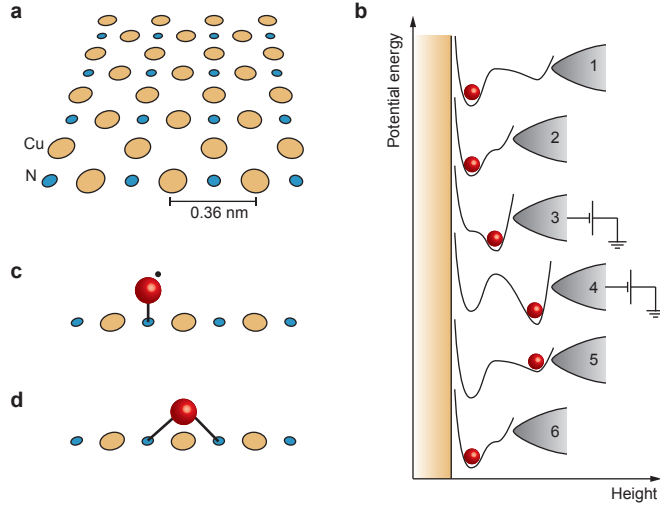


Figure 2. (a) Schematic showing the Cu_2N lattice: the orange circles represent Cu atoms while the blue circles are N atoms. The presence of strain on the underlying Cu(100) surface interferes in the growth process of the Cu_2N layer, that grows in islands, with typical sizes varying between 5 nm^2 and 20 nm^2 [41, 7]. (b) Visualization of pick-up and drop-off procedures for vertical atom manipulation. In all drawings, the left side of the double potential well represents the surface, the right side the tip. In (1) the tip is at imaging distance: the magnetic atom (red sphere) is stable on the surface. If the tip gets closer, the potential well is distorted (2). By applying a negative tip bias (the magnetic atom is positively charged), the right side of the potential well becomes more stable than the surface side and the atoms falls in (3). When the tip is then pulled away, the atom will move as well, as seen in (4). After restoring the imaging settings (5), the atom will stay on the tip side. When the tip is then moved closer to the surface, the atom will easily fall back to the surface (6). (c)-(d) Diagrams of the hopping process. In (c), the magnetic atom after being dropped off from the tip, is lying on top of a N atom with which it forms one valence bond (black line), leaving one electron unpaired. In (d), the Fe atom has hopped onto an adjacent Cu, and it is now forming two covalent bonds with the neighbouring N atoms. It is known from DFT calculations [4] that when an Fe atom is on top of a Cu, the latter is pushed down (lower than the neighbouring N atoms) and replaced in the lattice by the Fe.

the junction, so that when the tip is lifted up the atom follows [43, 44]. This whole process is possible due to the charging effect induced by the lattice on the magnetic atom: in the N–Fe–N bond, negative charges move away from the Fe atom towards the neighbouring N atoms, rendering the Fe atom positively charged. On the other hand, when the tip with an Fe atom at its apex is brought close to the surface, the shape of the potential well will favour the atom to move on the surface, even if only a very small positive tip voltage (or none at all) is applied.

When the magnetic atom is dropped off from the tip, the minimum energy configuration is for it to land on a N site of the Cu_2N lattice, forming a single covalent bond. However, in this way, one electron remains unpaired (figure 2c). As soon as a voltage pulse of approximately 1.1 V is applied to the Fe atom, it will move to an adjacent Cu site. In this new position, it will replace the Cu in the two-dimensional surface

network by pushing it down, and will form two covalent bonds with the neighbouring N atoms (figure 2d). In this new position, it is so strongly bound to the surface that the only way to move it again is via a new pick up. If, while applying the voltage pulse the tip is slightly offset away from the center of the atom in the direction of one of the four neighbouring copper atoms, the magnetic atom can be forced to jump in that particular direction, with reasonable reliability.

3.2. Inelastic electron tunnelling spectroscopy

The primary tunnelling process occurring in an STM configuration is elastic tunnelling, where no energy is lost by the electrons. But it is also possible for the electrons to tunnel inelastically. In this process, electrons give away energy during the tunnelling process leading to an additional transport path in addition to the regular elastic tunnelling path. This energy is absorbed by the environment in the form of e.g. a vibrational [45, 46] or magnetic [2] excitation. Since this excitation can occur only if the applied voltage exceeds the excitation energy, $eV > \Delta E$, the inelastic tunnelling path contributes to the conductance only beyond the excitation threshold. As a result, an inelastic excitation is seen in the differential conductance dI/dV as a sudden upward step at the onset voltage.

Differential conductance curves are commonly recorded at low temperature using lock-in detection at a frequency near bandwidth of the current amplifier (~ 1 kHz). The amplitude of the modulation signal gives an upper bound on the achievable energy resolution. Figure 3a shows a typical IETS spectrum measured on an Fe atom on Cu_2N . Apart from the onset energies for each of the excitations, in this case < 0.5 meV, ~ 4.0 meV and ~ 5.5 meV, which can be read off directly from the step positions, much more information can be extracted from this spectrum.

The *height* of each step gives the transition intensity for the corresponding excitation: it gives a measure for the quantum mechanical selection rules governing the spin excitations [4]. The intensity $I_{0 \rightarrow n}$, of the transition from the ground state $|\psi_0, \sigma_0\rangle$ to the n th eigenstate $|\psi_n, \sigma_n\rangle$, can be expressed as [47, 48, 49, 50, 51]:

$$I_{0 \rightarrow n} = |\langle \psi_n, \sigma_f | (\mathbf{S} \cdot \mathbf{s} + u) | \psi_0, \sigma_i \rangle|^2, \quad (1)$$

where the inner product of the spins \mathbf{S} of the atom and \mathbf{s} of the tunnelling electron, acting on their combined state, ensures that angular momentum is conserved: since the difference between the projections of σ_i and σ_f , the initial and final states of the tunnelling electron spin, can be no more than 1, neither can the difference between the ground state of the atomic spin ψ_0 and the targeted excited state ψ_n . This becomes immediately evident when we rewrite (1) as:

$$I_{0 \rightarrow n} = \left| \langle \psi_n, \sigma_f | \left(\frac{S_+ s_- + S_- s_+}{2} + S_z s_z + u \right) | \psi_0, \sigma_i \rangle \right|^2. \quad (2)$$

Note that the $S_z s_z$ term also allows elastic contributions (i.e. where $\psi_n = \psi_0$). In addition, the constant u represents an alternative elastic tunnelling path, possibly

through entirely different orbitals. The two elastic terms are referred to as ‘spin-dependent’ and ‘spin-independent’ elastic tunnelling respectively.

When we want to compare two dI/dV spectra taken on different atoms we need to normalize them; this is not a trivial issue. One could think of normalising them with current: every spectrum is recorded with the same initial current value at a specific bias voltage. However, the current is the integral of the dI/dV spectrum that we want to measure, and therefore the normalization of the measurement would always be influenced by the measurement itself. Also normalizing with respect to the tip height over an atom is not appropriate for the same reason: the apparent height is still related to the current and therefore the integral of the dI/dV . To avoid these problems, we choose to normalize the measurement on the bare Cu_2N : we set current and voltage on the substrate and then, without changing the tip height that stays fixed from the off-atom value, we move the tip on the atom that we want to measure and we can record the dI/dV spectra.

The *shape* of a step beyond the onset voltage, as can be seen on the negative voltage side in figure 3a, is not necessarily flat. Instead, in many cases the signal reaches a maximum after which it decays somewhat. Several causes can result in such nonlinear behaviour. First, saturation of the excited state may cause the inelastic signal to decline: beyond a certain voltage, above the excitation threshold, the population of the excited state becomes so high, and the population of the ground state so low, that gradually less is left to excite [51, 54].

The simulated IETS spectrum of a single Fe atom on Cu_2N is shown in figure 3a. The energies of the excitations follow directly from diagonalization of the total Hamiltonian of the system (13) that will be derived in section 4.2. The full dI/dV spectrum is modelled by using [55, 56, 4, 57]

$$\frac{dI}{dV} \propto \sum_n I_{0 \rightarrow n} \times \left[F\left(\frac{eV + \Delta E_n}{k_B T}\right) + F\left(-\frac{eV - \Delta E_n}{k_B T}\right) \right], \quad (3)$$

where the function F , defined as $F(x) = [1 + (x - 1) \exp x] / [\exp x - 1]^2$, gives the correct shape to the IETS steps (taking into account thermal broadening), while ΔE_n is the energy difference between the n th and the ground state and eV is the applied voltage.

As can be seen in figure 3a, the dI/dV curve simulated with (3) cannot reproduce the aforementioned nonlinear behaviour previously identified in the negative voltage side of the Fe spectrum. Whether saturation is the dominant reason for the nonlinear lineshape can be checked by reducing the total current (i.e. by increasing the tip height): when the (inelastic) current is smaller, saturation should be reached at a larger voltage and the decay becomes less steep. In this case, those lineshapes can be reproduced by taking into account also secondary transitions that start from an excited state. This can be done with the use of Pauli Master equations [51, 53]. In this method, the time evolution of every state is calculated taking into account the total transition rate into and out of that state, considering all possible spin contributions to the the total rate.

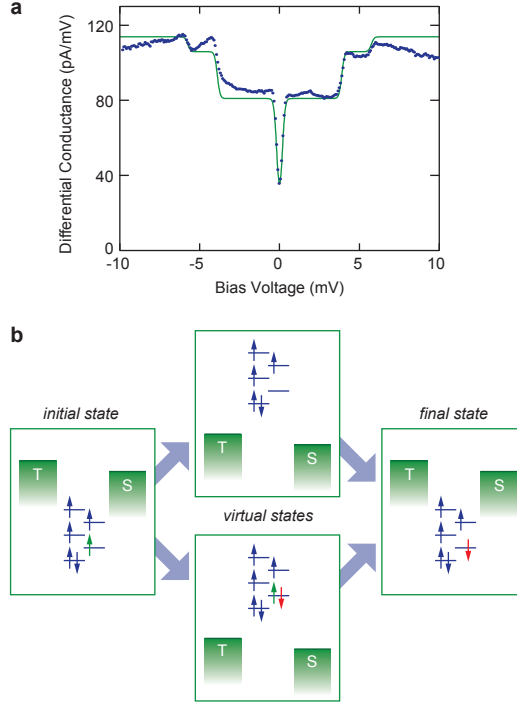


Figure 3. (a) dI/dV spectrum (dark blue), and correspondent simulated curve (green) of a single Fe atom on $\text{Cu}_2\text{N}/\text{Cu}(100)$, in absence of external magnetic field and at 330 mK. The steps are the inelastic spin excitations from the ground state. (b) Schematic of an inelastic cotunnelling process behind an STM measurement. In the initial configuration, the magnetic atom is in the ground state; in the final configuration, one spin has been flipped. This can happen in two possible virtual ways: a hole (a) or an electron (b) can tunnel to the magnetic atom without conserving the energy (the magnetic state is now outside the energy range of the two sides of the tunnel junction), and at the same time another hole or electron can tunnel from the magnetic atom to the other side of the barrier. In this way the system has changed its magnetization. The reason why it is possible to have this process, is that the time spent from the system in the virtual state (without energy conservation) is the Heisenberg uncertainty time $t_H \simeq \hbar/E_C$, with E_C the energy that the system should have paid to have a real excitation to the intermediate state [52, 53].

Moreover, this saturation effect can be used to measure the lifetime of the excitation: by analysing the lineshape we can determine what magnitude of inelastic current is needed to compete with the relaxation process. With this method, the lifetimes of the excited states of individual Mn atoms on Cu_2N were found to vary between 0.1 ns and 1.0 ns [51].

In other situations, nonlinearities in the IETS spectra are not caused by saturation and persist even for small currents. In these cases, higher order terms need to be taken into account in the description of the tunnel current. Very similar lineshapes can be caused for instance by higher order effects due to the Kondo interaction of the atom with the bulk conduction electrons [58, 59], as will be explained in section 4.3.

Finally, the *width* of the steps is a measure for thermal (or modulation) broadening of the IETS signal or due to lifetime broadening of the spin states, whichever of the two is largest. Since spin lifetimes on Cu_2N are in the order of 0.1 ns or longer, measurements performed at typical temperatures of ~ 1 K or higher will be dominated by thermal broadening. Spin excitation IETS has been observed in various other systems, including molecular magnets [60, 61], magnetic dopants in semiconductors [62] and magnetic atoms on metal substrates [6].

As a transport phenomenon, inelastic tunnelling is well described in terms of cotunnelling in the Coulomb blockade regime [53, 63]: a framework that is used very successfully in the field of quantum transport through quantum dots [64, 65, 66]. In cotunnelling, the energy levels between which excitations are made are assumed to be well outside the energy window defined by the applied bias voltage (figure 3b). Spin-flip excitations involve temporary virtual double occupancy (or de-occupancy) of orbitals that are singly occupied when at rest.

3.3. Functionalized spin-polarized tips

The invention of the Scanning Tunnelling Microscope in the early 1980s has revolutionized the study of conductive material surfaces. However, the first proposal for implementing the STM to observe spin-contrast, and therefore atomic-scale magnetism, was produced only at the end of the decade by Pierce [67]. The principle of a spin-polarized (s-p) STM is to read the polarization of the surface spins with the tunnelling electrons provided by the tip, that have to be spin-polarized as well. The resulting conductance will depend on the overlap of the polarized electron states in both tip and sample.

The simplest of the methods proposed by Pierce was to create a polarized tunnelling current using a magnetic tip. The first spin-polarized STM experiment [68] was performed with a ferromagnetic CrO_2 tip, that was used to get a topographic contrast of the antiferromagnetically ordered Cr terraces of a (100) surface. The apparent height of the atomic steps was different if the tip and the surface polarizations were parallel or not, allowing to obtain nanoscale magnetic resolution. The development of new methods to prepare sharper tips, allowed soon to achieve atomic spin contrast: in Ref. [69] it is shown for the first time magnetic imaging at the atomic level, using a very sharp Fe tip to image a magnetite sample. After this improvement, the field of s-p STM has produced many studies of atomic scale magnetism using magnetic or magnetically coated tips, like e.g. Refs. [70, 71, 72] in the first decade of 2000 (other examples can be found in the review papers [73, 74]), or more recently [75, 20].

Another method to achieve a spin polarized STM tip is to start with a nonmagnetic tip, and prepare it *in situ* by transferring material from the magnetic surface to the tip, creating a magnetic cluster on the tip apex to make it sensitive to the spin orientation. One way of doing this is by applying voltage pulses [76]: this was shown to cause mass transport from sample to tip and to vary the magnetization direction of the STM tip.

Alternatively, the tip can be indented into the magnetic substrate to obtain the same effective coating [77]. These methods are easier to achieve than coating a non magnetic tip with a thin film of magnetic material [74].

After the invention of vertical atom manipulation, this last technique to polarize the STM tip could be performed in a controlled way. It was demonstrated that if a single magnetic atom is picked up from the surface with a non magnetic tip and replaces the tip apex, the tip becomes a paramagnet [57, 51]. When an external magnetic field $\mathbf{B} \sim 100$ mT is applied, due to the Zeeman effect the tip will acquire a spin-polarization parallel to \mathbf{B} . This method enables to switch very easily from a non-magnetic tip to a s-p one, allowing to measure the same atom with or without spin contrast [22].

Tersoff and Hamann [78, 79] have theoretically related the experimentally measured tunnel current and the electronic states of both tip and sample, starting from the perturbative approach introduced by Bardeen [80]. Without going into mathematical details, that can be found for instance in Ref. [74], they found an exponential dependence of the current on the distance between tip and sample \mathbf{d} :

$$I_0(\mathbf{d}) \propto \exp(-2\kappa\mathbf{d}). \quad (4)$$

This well-known relation is valid only for a non polarized tunnel junctions, since it is based on the assumption that the tip wavefunction is of the s -type. As soon as a tip polarization is introduced, the current needs to be corrected to properly take it into account. It can be expressed as [74]:

$$I_{SP}(\mathbf{d}) \propto I_0(\mathbf{d}) [1 + P^T P^S \cos\beta], \quad (5)$$

where $I_0(\mathbf{d})$ is the non polarized tunnel current (4) that exponentially depends on the distance \mathbf{d} , β is the angle between tip and sample polarization directions, and $P^{T,S}$ are the polarizations of respectively tip and sample, defined as (α can be either tip or sample):

$$P^\alpha = \frac{n_\uparrow^\alpha - n_\downarrow^\alpha}{n_\uparrow^\alpha + n_\downarrow^\alpha}, \quad (6)$$

with n_\uparrow^α and n_\downarrow^α being the spin-resolved densities of states for the two magnetic electrodes.

This difference in current between states with opposite magnetization directions, can be visualized as apparent tip height variation when imaged in constant-current mode. In figure 4 we show a topographic image of an antiferromagnetic structure composed of 15 Fe atoms on a Cu_2N lattice, with spacing similar to the structures presented in Ref. [19]. The apparent high-low pattern among the atoms is an indication of the antiferromagnetic coupling in the structure: since the tip is polarized in the same direction as the atoms on the surface, an atom that looks higher is magnetized in a parallel alignment to the tip apex, while an atom that looks lower is in an antiparallel configuration. We note that since the number of atoms in the structure is odd, the shown Néel state is stable. For an even numbered case, the stability depends on the number of coupled atoms [19], as will be explained in section 5.

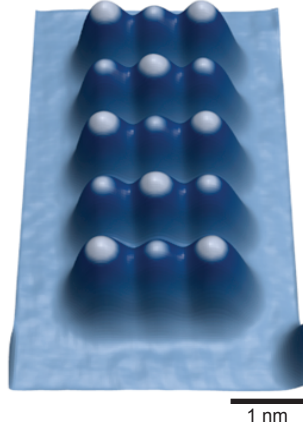


Figure 4. Antiferromagnetic structure composed of 15 Fe atoms on a $\text{Cu}_2\text{N}/\text{Cu}(100)$ substrate, imaged with a spin polarized tip. A magnetic field $B = 1$ T is applied in plane, parallel to the easy axis direction of the Fe atoms, to polarize the tip. The apparent height difference between the atoms is $\Delta y = 15$ pm. This structure is similar to the antiferromagnetic arrays presented in Ref. [19].

4. Modelling the environment

In the previous section we have seen how spin excitations appear as steps in an IETS measurement. Now we will focus on the physics of the spin states themselves. In our experiments on Cu_2N , the atomic spin's excitation energies are governed by three factors, all working on comparable energy scales: (i) magnetic anisotropy, (ii) the Zeeman effect and (iii) Heisenberg interaction with neighbouring atoms.

4.1. Magnetic anisotropy

When a magnetic atom is embedded inside a crystal structure (or placed on top of a crystalline surface), broken symmetries between the different crystallographic axes may lead to some orientations of the magnetic moment being favoured over others: the primary ingredient for magnetic stability. This breaking of symmetry stems from the electrostatic potential of the crystal lattice having a different effect on each of the partially filled d-orbitals (for transition metals), in which the atom's net magnetic moment resides.

If this crystal field splitting is to such a degree that no degeneracy between any two d-orbitals remains, no electron can be in a state that has a considerable finite expectation value for the orbital angular momentum \mathbf{L} , for which always a linear combination of two orbitals is needed, and we say that the orbital momentum has *quenched*. In such cases, the total magnetic moment of the atom is best described by \mathbf{S} , the combined spin momenta of the atom's uncompensated electrons. Whatever remains of \mathbf{L} is felt by this spin \mathbf{S} through the spin-orbit coupling $\lambda \mathbf{L} \cdot \mathbf{S}$ as a small perturbation (λ is the spin-orbit constant). Depending on the orientation of \mathbf{S} with respect to the orbitals this may lead

to either an energy gain or loss, giving rise to magnetic anisotropy.

Traditionally, the magnetic anisotropy is quantified by the anisotropy Hamiltonian [81]

$$\mathcal{H}_{\text{aniso}} = DS_z^2 + E(S_x^2 - S_y^2), \quad (7)$$

where D and E are respectively the uniaxial and transverse anisotropy parameters. By definition, D corresponds to the magnetic orientation whose anisotropy energy stands out most (either in a positive or a negative way), while E gives the energy difference between the remaining two orientations. For example, if $D < 0$ and $E > 0$, it follows that z is the easy axis, y the intermediate axis and x the hard axis.

In the ideal case where $E = 0$ and $D < 0$ (easy axis uniaxial anisotropy), the energy landscape of the spin takes the shape of a parabola with height DS^2 (S being the magnitude of \mathbf{S}) separating magnetization eigenstates $|m_z\rangle = |-S\rangle$ and $|m_z\rangle = |S\rangle$. Since the S_x and S_y operators do not commute with S_z , the presence of a small transverse anisotropy E will lead to mixing of the states. For an integer spin system this results in the two lowest states becoming symmetric and antisymmetric superpositions of $|-S\rangle$ and $|S\rangle$. In this case it is possible for the magnetization to tunnel from one orientation to the other and magnetic stability is lost. Only when a magnetic field $E/\mu_B \ll \mathbf{B} \sim DS^2/\mu_B$ (μ_B being the Bohr magneton) is applied along the z -direction do the states sufficiently separate again to form a bistable system; for higher fields, the state fully aligned to \mathbf{B} becomes highly favourite.

For half-integer spins there is also mixing of states, but not within doublets due to Kramers' theorem [82]. This can be easily seen when we rewrite the anisotropy Hamiltonian in terms of the spin raising and lowering operators S_+ and S_- :

$$\mathcal{H}_{\text{aniso}} = DS_z^2 + \frac{E}{2}(S_+S_+ + S_-S_-), \quad (8)$$

which can only couple states whose m_z values are a multiple of 2 apart. Instead, half-integer spins with transverse anisotropy can tunnel from e.g. $|-S\rangle$ to $|S-1\rangle$ or from $|-S+1\rangle$ to $|S\rangle$.

The representation in terms of D and E becomes inconvenient whenever E approaches $|D|/3$. As shown in figure 5a and figure 5b, a small variation in the anisotropy energy of e.g. the y -orientation may lead to a situation where D changes sign, switching from an easy axis to a hard axis configuration or vice versa, and all the axes need to be rearranged. One could decide not to invert D and leave the axes unchanged (i.e. to abandon the requirement that D always corresponds to the orientation that stands out most) but this would lead to the possibility of multiple combinations of D and E describing the same anisotropy configuration, which is even less desirable. A second disadvantage of this representation is that the D and E parameters are only phenomenological and do not provide much insight into the origin of anisotropy as a result of spin-orbit coupling.

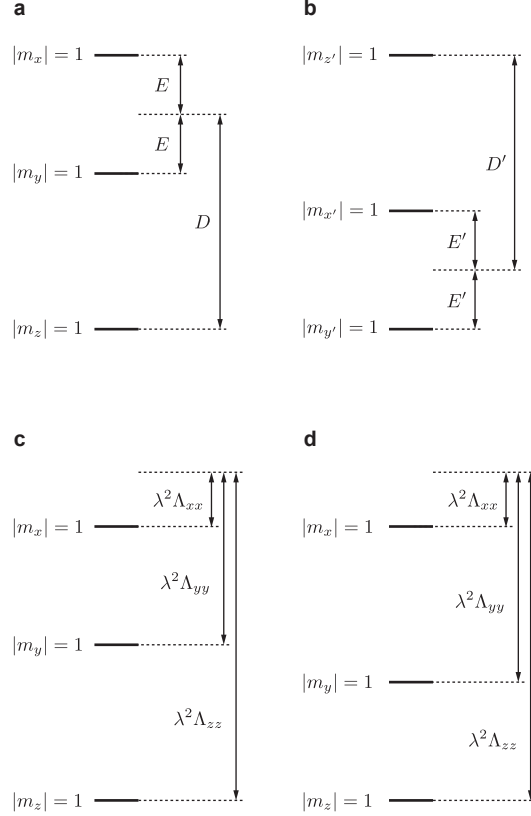


Figure 5. (a) Energy diagram for a $S = 1$ system being fully aligned along the x , y and z axes, with easy axis anisotropy ($D < 0$) and a transverse anisotropy E which is just smaller than $|D|/3$. (b) Similar to (a), but with E just larger than $|D|/3$, calling for new anisotropy parameters D' and E' as well as rearranged axes x' , y' and z' . (c),(d) Same situations as in (a) and (b), but now represented in terms of Λ . The dashed line representing zero energy here is arbitrary: a random identical offset can be added to each of the $\Lambda_{\mu\mu}$ parameters as long as they all stay positive.

For both these reasons, it is convenient to switch to a representation in terms of the anisotropy tensor Λ , whose elements are the matrix elements of the orbital momentum in second order perturbation theory [83]:

$$\Lambda_{ij} = \sum_{n \neq 0} \frac{\langle \psi_0 | L_i | \psi_n \rangle \langle \psi_n | L_j | \psi_0 \rangle}{E_n - E_0}. \quad (9)$$

Here the states ψ_n refer to different orbital filling configurations with ψ_0 the ground state configuration. In a case of a high-symmetry crystal environment, all the off-diagonals of Λ are typically zero, leaving only [84]:

$$\Lambda_{\mu\mu} = \sum_{n \neq 0} \frac{|\langle \psi_0 | L_\mu | \psi_n \rangle|^2}{E_n - E_0}, \quad (10)$$

with $\mu = x, y, z$. In terms of these matrix elements the anisotropy Hamiltonian can be rewritten as:

$$\mathcal{H}_{\text{aniso}} = -\lambda^2 (\Lambda_{xx}S_x^2 + \Lambda_{yy}S_y^2 + \Lambda_{zz}S_z^2) \equiv -\lambda^2 \sum_{\mu=x,y,z} \Lambda_{\mu\mu}S_{\mu}S_{\mu}. \quad (11)$$

In this form the Hamiltonian is very easy to read: whichever $\Lambda_{\mu\mu}$ is largest simply corresponds to the easy axis while the smallest $\Lambda_{\mu\mu}$ corresponds to the hard axis. In addition, as shown in figures 5c–d, there is no longer the need to rearrange the axes when the system switches between easy axis and hard axis configurations.

One could say that $\Lambda_{\mu\mu}$ represents the extent to which L_{μ} , the component of the orbital angular momentum in the μ -direction, is *unquenched*. Of course, this quantity can never exceed L , the magnitude of \mathbf{L} . When the energy difference between two states ψ_n becomes too small, $\Lambda_{\mu\mu}$ will rapidly increase and the approach of treating the spin-orbit coupling as a perturbation breaks down. In this case the anisotropy energy can be read off directly from the $\lambda\mathbf{L} \cdot \mathbf{S}$ term in the Hamiltonian. From this it can be seen that the maximum height of the anisotropy barrier, i.e. the maximum difference in energy between to perpendicular orientations of \mathbf{S} , can never exceed λLS .

4.1.1. Strain induced variation of magnetic anisotropy The Hamiltonian (11) now expresses the magnetic anisotropy in terms of physical parameters. Using this notation makes it is easier to understand the significant variations in anisotropy measured in some cases. In Ref. [5], three different types of Fe dimers were built via vertical manipulation. These pairs of atoms were chosen such that they all have the same separation distance in terms of Fe–N and Cu–N bonds, but their precise geometries were different. Inelastic tunnelling spectra were recorded on every atom of the dimer: for pairs in which the second atom was along (or within one bond length of) the easy axis of the first atom, an enhancement of the magnetic anisotropy, with respect to the isolated Fe atom value, was measured. On the other hand, when the second atom was further away from the easy axis, a decrease in the magnetic anisotropy was found.

A model was developed to explain the observed results, based on the action of strain induced by the presence of the second atom, that changes the local crystal field. Of the three different instances of dimers described in Ref. [5], only the more instructive one, shown in figure 6a, will be discussed here. This is the building block of the magnetic bistable structures presented in Ref. [19]; the two Fe atoms are positioned along a N-row of the Cu_2N network, spaced two unit cells (0.72 nm apart), and for both atoms a significant increase of the magnetic anisotropy is detected.

As seen in section 3.1, a single Fe atom on Cu_2N binds on a Cu site. According to DFT calculations the Fe atom pushes this Cu atom down into the bulk and replaces its position in the surface molecular network [4]. The Fe atom forms two covalent bonds with the neighbouring N atoms, that are slightly pushed downwards as well, thus constituting a N–Fe–N structure. If this structure is linear, the corresponding crystal field is linear as well, and the produced splitting of the Fe d -orbitals is shown in

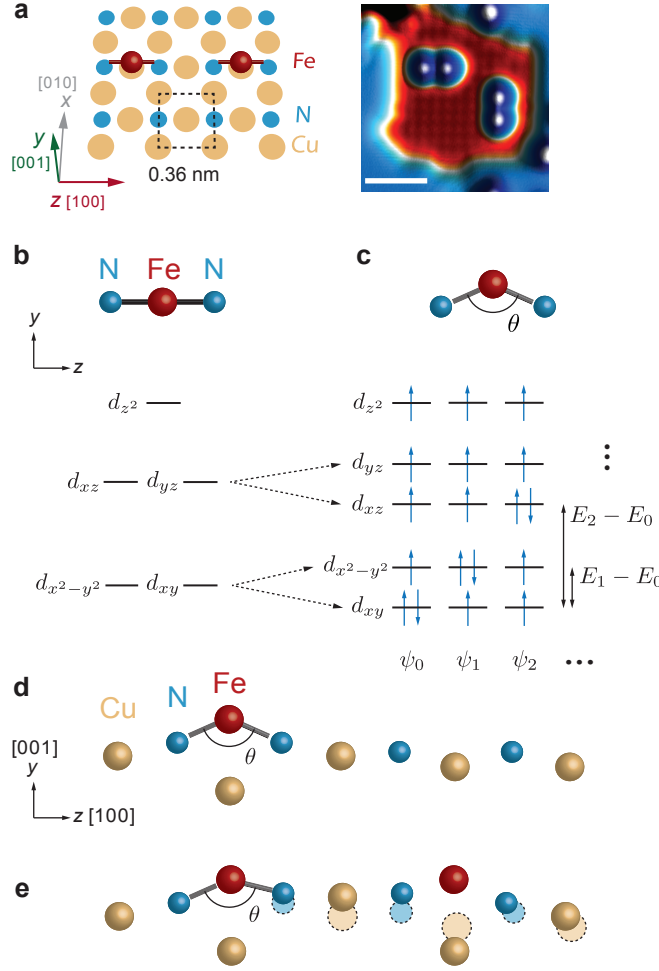


Figure 6. (a) Diagram and STM topographic image of two instances of the linear dimer. Red bars indicate the magnetic easy axis along a nitrogen row. The unit cell of Cu₂N is also shown. Scale bar in topography is 2 nm. (b) Proposed splitting of the d -orbitals resulting from a linear field. (c) Same as (b) but for a C_{2v} crystal field ($\theta < 180^\circ$). Now all the orbital degeneracies have been lifted. The orbital configurations for the three lowest energy orbital states ψ_n are shown. (d) Schematic of a single Fe on Cu₂N. (e) Same as (d) but for the linear dimer: the presence of the second atom lifts the central Cu atom, in this way increasing θ . The dashed outlines show the corresponding lattice displacement in the case of a single Fe atom. All panels edited from Ref. [5].

figure 6b. However the crystal field created by this environment is not linear, but has a C_{2v} symmetry, caused by the presence of the angle θ in the N–Fe–N bond. The result of this symmetry is that all the degeneracies between the orbital eigenstates are lifted (figure 6c).

The anisotropy parameters $\Lambda_{\mu\mu}$, as defined in (10), are inversely proportional to the energy difference between those states. In particular, Λ_{zz} , the amount of unquenched orbital momentum along the nitrogen direction of the lattice (z -direction), is inversely proportional to $E_1 - E_0$, the energy difference between the ground state and the first

orbital excited state. This energy difference will vanish in the limit of $\theta = 180^\circ$ in the N–Fe–N bond. The other two components of the anisotropy tensor will depend on the energy differences $E_2 - E_0$ and $E_3 - E_0$, that are less strongly influenced by the angle θ .

In figure 6d a schematic, based on DFT calculations, of a single Fe atom embedded inside a Cu_2N lattice is shown: the neighbouring N atoms and the next-nearest-neighbour Cu atoms are lifted and move toward the Fe atom. When a second Fe atom is placed along the same lattice row, it will lift the neighbouring N atoms, like the first Fe (figure 6e), and the central Cu atom will be raised more, since it is now interacting with both Fe atoms. As a consequence, the angle θ will increase, resulting in an enhancement of Λ_{zz} . To summarize, the presence of the second atom has induced strain on the lattice that has modified the local crystal field felt by the single Fe atom, and therefore the splitting within its d -orbitals, leading to a significant variation of the magnetic anisotropy.

Analogous reasoning can be made to explain all observed variations between different dimer geometries. The dimer discussed here, however, since it is built along a nitrogen row of the lattice, is the one most sensitive to variations in strain: it is in a critical regime in which even the smallest modification of the angle θ can induce a very large variation in the magnetocrystalline anisotropy. Comparable results were found for Co pairs on Cu_2N [59]. Also in this case, the dimer built with the same geometry was the most sensitive to strain and produced the largest variation in anisotropy compared to isolated atom value.

4.2. Heisenberg interaction

If two or more magnetic atoms are placed on a surface at a close distance, their electrons will interact. This interaction can be direct, like in the formation of a covalent bond [85], but it can also be indirect: mediated by a non magnetic atom, commonly known as superexchange interaction [86], or mediated by the delocalised electrons of a conducting material (Ruderman-Kittel-Kasuya-Yosida or simply RKKY interaction) [87, 88, 89]. Both these interactions are collinear, favouring either parallel or antiparallel alignment of the spins. Until now, no clear picture has emerged as to which of the two interactions dominates for magnetic atoms on Cu_2N . In none of the experiments evidence of non-collinear interaction, such as Dzyaloshinskii-Moriya as found in magnetic surfaces [71], have been reported.

The strength of the interaction can be tuned by changing the relative positioning of the atoms on the lattice [5]. We can model their magnetic interaction using the Heisenberg exchange Hamiltonian [47]:

$$\mathcal{H}_{\text{Heis}} = \sum_{i,j} J_{ij} \mathbf{S}_i \cdot \mathbf{S}_j, \quad (12)$$

with the sign of J defining whether the coupling is ferromagnetic (FM, $J < 0$) or antiferromagnetic (AFM, $J > 0$). In our system we find that it is generally sufficient

to consider only interactions between nearest neighbours, therefore limiting the sum to $j = i + 1$.

If we consider all the different contributions, we can write the total Hamiltonian for a system composed of N magnetic atoms on a surface, coupled within nearest neighbours with strength J and in presence of an external magnetic field \mathbf{B} (μ_B being the Bohr magneton):

$$\mathcal{H} = JS^i \cdot \mathbf{S}^{(i+1)} - \sum_{i,\mu} [\lambda^2 \Lambda_{\mu\mu} S_\mu^i S_\mu^i + 2(1 - \lambda \Lambda_{\mu\mu}) \mu_B B_\mu S_\mu^i], \quad (13)$$

where the index i refers to the i -th atom in the structure. We point out that when expressing the spin-orbit interaction in terms of the $\Lambda_{\mu\mu}$ parameters, the g -factor becomes a tensor [83, 84].

IETS spectra taken on a coupled spin system look different from the spectrum recorded on an isolated atom. The STM tip is in fact probing the collective spin excitations of the combined system: the number of possible excitations increases with the number of atoms. Local selection rules as determined by (1) determine which excitation appears on which atom. Depending on the coupling strength, different regimes can be discerned. If the coupling is very strong compared to the other energy scales of the problem, spectra recorded on different atoms look exactly the same. This is the case for Mn chains built on Cu_2N along the nitrogen row and at the close spacing of 0.36 nm [15]. On the other hand, if the coupling is very small, the spectra look very similar to the single atom, with the coupling acting like a small perturbation [13, 57]. In the intermediate regime, when the coupling strength is comparable to the anisotropy and the Zeeman term, the spectra look all different to each other but present a collective behaviour, as shown for a ferromagnetically coupled Fe chain [22]. In fact, the first excitation for every atom is at the same energy and has the same intensity, including the outer atoms of the chain that have only one neighbour. For higher energies, the excitations have a different intensity depending on the atom position along the chain, in a manner consistent with spin waves as will be clarified in section 5.2 and figure 8.

4.3. Kondo screening

The Kondo effect is a many-body interaction between a single magnetic atom and a non-magnetic metal. In the simplest picture (Anderson impurity model [90]), the magnetic impurity has only one electron that can be exchanged with the electron bath via a virtual process [91]. The minimum energy configuration corresponds to the formation of a spin singlet (the Kondo state) between the localized moment and the net spin of the electron bath, that screens the spin of the magnetic impurity. As a result, a sharp resonance peak appears in the electron density of states (DOS) at the Fermi energy.

Jun Kondo [92] used this model to explain a non-conventional behaviour of the electrical resistance, that was observed for the first time during the 1930s [93]. For a normal metal, the resistance drops with decreasing temperature, and saturates below ~ 10 K, reaching a value that depends on the concentration of defects in the metal.

However, in the 1930s experiment, the resistance of a gold sample was found to decrease with temperature up to a minimum value, while for even lower temperatures it started to increase again. Kondo associated this anomalous increase in the resistivity with the presence of magnetic impurities in the metal and the consequent formation of a Kondo resonant state. This happens below a characteristic temperature, the Kondo temperature T_K , that depends on the coupling strength between the impurity and the electron bath [91].

The development of experimental tools in nanoscience has opened the doors to new approaches in the study and control of this phenomenon, that before could only be indirectly observed via resistance or magnetic susceptibility measurements. Since 1998 nanotechnologies have made possible to probe a single Kondo impurity: quantum dots [94, 95] and carbon nanotubes [96] have allowed to create externally controllable Kondo systems, while the STM has been used to study the interaction between magnetic atoms on top of metal surfaces with atomic resolution [8, 97].

The signature of the Kondo effect in an STM measurement is the appearance of a resonance peak at zero voltage in the IETS spectrum for temperatures lower than T_K . When a magnetic atom is deposited directly on top of a metal the interactions with the conduction electrons are very strong, giving rise to a Kondo temperature in the order of 30–100 K [98, 9]. The Kondo interaction, and as a consequence T_K , is reduced if there is a decoupling layer like Cu_2N separating the magnetic atom from the bulk substrate [2]. For example, for Co atoms on Cu_2N , the Kondo temperature is found to be $T_K = 2.6 \pm 0.2$ K [11].

In order for a spin to be Kondo screened, a single electron from the bath needs to be able to flip the impurity spin. Therefore, its ground state needs to fulfil certain criteria: it needs to be at least twofold degenerate, and the magnetization m of two degenerate ground states needs to differ by $|\Delta m| = 1$. For this reason not all magnetic atoms will be Kondo screened when placed on a metal; known examples observed with an STM are Co [8, 99, 98], Ce [97], Ti [100] and Ni [101] atoms on $\{111\}$ and $\{100\}$ surfaces of Cu, Ag and Au.

Fe on Cu_2N has a spin $S = 2$ and a negative anisotropy parameter D , so the two lowest states are in the subspace of $|m_z\rangle = |2\rangle$ and $|m_z\rangle = |-2\rangle$, which differ by $|\Delta m| = 4$. In addition, the presence of the transverse anisotropy term E breaks the degeneracy between the states, causing neither of the two criteria for Kondo screening to be met. Co atoms on the other hand, have a spin $S = 3/2$, but $D > 0$, so the lowest energy states have $m_z = 1/2$ and $m_z = -1/2$. This makes Co a good candidate for Kondo screening. IETS spectra measured on a single Co atom on Cu_2N show a sharp resonance peak at zero voltage [11].

5. Magnetic bistability

As we have seen, a single magnetic atom may exist in a superposition of two magnetization states despite, or even because of, the presence of strong anisotropy. Yet,

bulk magnetic materials consisting of many interacting atoms do become magnetically bistable. The ability of our experiments to control the number of atoms in the system, as well as the anisotropy and the coupling strength, provides a unique opportunity to observe and investigate the emergence of classical magnetic bistability with increasing atom number.

In systems with easy axis anisotropy, two metastable energy minima are separated by an energy barrier providing stability to two opposite spin orientations [102, 103]. Several effects may work to reduce this stability. First, thermal excitations may overcome the barrier, or a strong enough external magnetic field may make the barrier sufficiently asymmetric to destabilize one side. Also electron-induced excitations (caused e.g. by interactions with substrate electrons or tunnelling electrons in the case of an STM experiment) can allow the system to gain energy and climb the ladder of states to reach the other side. But even at very low temperatures and in the absence of a magnetic field or electron excitations, quantum tunnelling of magnetization can allow the system to go directly from one state to the other in case finite overlap between the states exist [104, 105].

With the miniaturization of memory storage devices reaching levels where quantum effects can no longer be neglected, control of the magnetic stability at the atomic scale is becoming a topic of increasing interest. Bistable behaviour has been reported in several systems composed of only several atoms, e.g. Fe nanoislands on W(100) [106, 107] and Co chains on Pt [108]. More recently, spin-polarized STM experiments have revealed switching between magnetic states on spin structures built through atom manipulation [19, 20], and have shed light on the spin dynamics during a magnetic switch [22]. In 2013 bistability was reported on individual rare-earth atoms deposited directly on a metal [21]. Very recently it was demonstrated by means of electronic pump probe spectroscopy [109] that stability in small structures built on Cu_2N can be modified via exchange interaction with the tip [110].

In the example of Loth et al. (2012) [19], construction of antiferromagnetically coupled Fe chains on $\text{Cu}_2\text{N}/\text{Cu}(100)$ resulted in bistability. By creating eight arrays of (2×6) Fe atoms, the authors were able to build the first atomic byte and store information in it for hours, providing a significant advancement towards the creation of nanoscale memory storage devices. In the case of an antiferromagnet, the two lowest energy states are the two classical Néel states, in which the spins are counter-aligned to form a collective state with zero net magnetization. In this experiment it was observed current and temperature induced switching between the Néel states. Moreover, the intrinsic (i.e. temperature independent) switching rate, that the authors attribute to quantum tunnelling of magnetization, was found to depend very sensitively on the number of atoms in the structure: by adding just two atoms to a six-atom chain, the intrinsic switching rate reduced by three orders of magnitude.

An antiferromagnetic system is a relatively complex magnetic object: technically, neither of the Néel states is ever an eigenstate of the system. In order to better understand the spin dynamics during a magnetization reversal, it may therefore be

easier to study a ferromagnetic system, as shown in Ref. [20]. Here, the authors studied the magnetic switching of a cluster of Fe atoms, built directly on a metal Cu(111) substrate, ferromagnetically coupled to each other. Unfortunately, due to the short-range coupling between the iron atoms, this system could not be probed or excited with single spin resolution. In Ref. [22], bistability in ferromagnetically coupled Fe structures on Cu₂N, enabling larger atom separation, was achieved.

In section 5.1 we will present methods to detect magnetic switching, including arrangements to measure regimes that are too fast or too slow for conventional detection. Next, in section 5.2 we will investigate the role played by stationary spin waves, confined into a ferromagnetic Fe chain, to revert its magnetization. Finally, in section 5.3 we will present novel switching data on antiferromagnetic structures that may be used to extract information about the spin polarized the STM tip.

5.1. Telegraph noise detection

Magnetic bistability can be detected by making the magnetic structure interact with a spin polarized STM tip. In the resulting magnetic tunnel junction, the measured conductance will be higher when the spins of tip and sample are in parallel alignment to each other and lower when they are antiparallel. If an atom or a structure is switching between two magnetization states, the tip will measure a current (and therefore conductance) that is alternating stochastically between two different values, corresponding to the two different configurations, that we call high-current G_H and low-current G_L . If the measurement is performed in constant-current mode, the switching behaviour of the current can be observed as a switching behaviour of the tip height. An example trace of this telegraphic noise signal is shown in figure 7a.

In order to estimate the switching rates between the two states, those telegraph noise curves need to be recorded for enough time to detect a statistical number of switches. Between switches, the system spends a time interval in a specific state; by making a histogram of the different time intervals spent by the system in one state, we observe an exponential decay. We can at this point extrapolate the Poissonian lifetime of each state from the two exponential decay times, and the inverse of the lifetimes are a measurement of the switching rates. This procedure is shown in figure 7b.

When the switching rate exceeds the bandwidth of the current amplifier, for example when a small structure is measured or when a larger bias voltage is applied, a pulsed measurement scheme can be used as shown in figure 7c [19, 22]. The idea is to apply a voltage larger than the threshold for inelastic excitations in very short pulses, on top of a DC voltage below the threshold. It is assumed that the probability for a switch to occur in the low-voltage intervals is zero. In these time intervals the magnetization can be considered frozen. As a result, one can say that the amount of relevant time passed in a time interval Δt is $\Delta t(t_1/(t_0 + t_1))$, where t_1 and t_0 are the pulse length and the zero voltage interval respectively. In other words, the measurement time has slowed down with respect to real time by a factor $t_1/(t_0 + t_1)$, allowing much faster switching

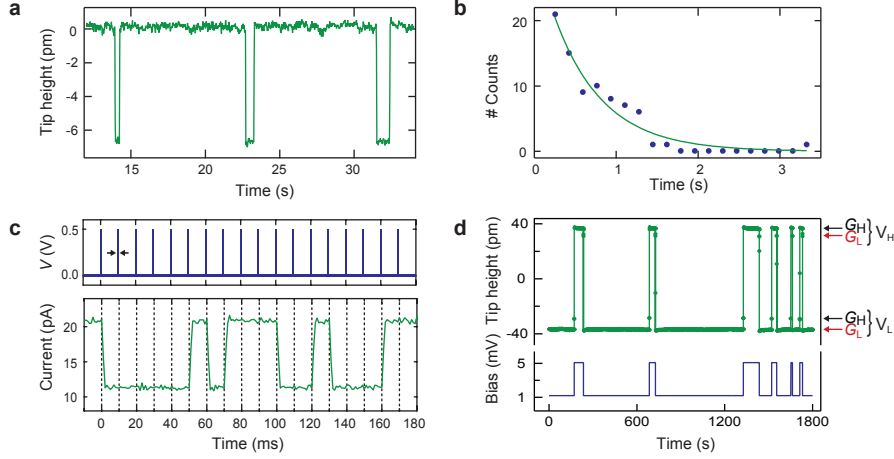


Figure 7. (a) Part of a constant-current switching trace, recorded for the second atom of a chain composed of 6 Fe atoms ferromagnetically coupled to each other. It was recorded with sample bias voltage $V = 3.7$ mV (above the 3.5 mV threshold for inelastic excitations), current $I = 20$ pA, magnetic field $B = 200$ mT and temperature $T = 330$ mK. (b) Time histogram (blue markers) corresponding to the full switching trace from G_L to G_H of panel (a). From the exponential fit (green curve), the lifetime of the low current state can be extracted as the decay time. (c) Example of a pulsed measurement, taken from [19]. The top part shows the voltage pulses, 10 ns long, and below the corresponding response of the system. (d) Feedback mechanism to measure very slow switching rates, developed in [22]. As soon as a switch from G_H to G_L is detected in the V_H state, the bias is suddenly lowered, with the system still in G_L but at low bias (below threshold). When the system switches back to G_H , the bias voltage is set back to the high value.

processes to be investigated.

On the other hand, in some cases the switching rate can be extremely slow. If the system is a ferromagnet, it will spend most of its time in one state, even if the applied field (required for magnetizing the SP tip) is very small. As a consequence, in order to obtain enough statistics to extract lifetimes, a way to speed up the process needs to be found. An example is given in Ref. [22], in which a feedback mechanism is used as shown in figure 7d. If the system spends most of its time in state G_H , the switching rate from G_H to G_L is very slow. So to speed up the measurement, the (slow) rate from G_H to G_L is measured at a high voltage V_H (above inelastic excitation threshold), while the faster rate from G_L to G_H is measured at low voltage V_L (below threshold). As soon as a switch from G_H to G_L in the high voltage state V_H is recorded, the voltage is suddenly reduced to V_L , with the system ending in state G_L at low bias voltage. Then, when a switch to G_H is detected, the voltage is restored to V_H . This method enables measurement of the intrinsic switching rate from the unfavoured to the favoured state, without having to wait endlessly while the system spends time in the favoured state.

5.2. Spin wave mediated reversal

Very recently, in Ref. [22] real-space atomic scale imaging of standing spin waves was reported. The spin waves were confined inside an artificial ferromagnet containing only six Fe atoms. In this experiment, the possibility to have ferromagnetic coupling between Fe atoms over relatively large distance on Cu_2N [5], enabled to study the collective excitations of the structure while addressing each atom individually. By using a combination of spin polarized STM to detect the magnetic switching, and IETS to characterize the inelastic excitations, the authors were able to study the complex spin dynamics that governs the magnetization reversal of a ferromagnet. In this section we will focus on the role played by spin waves during this process.

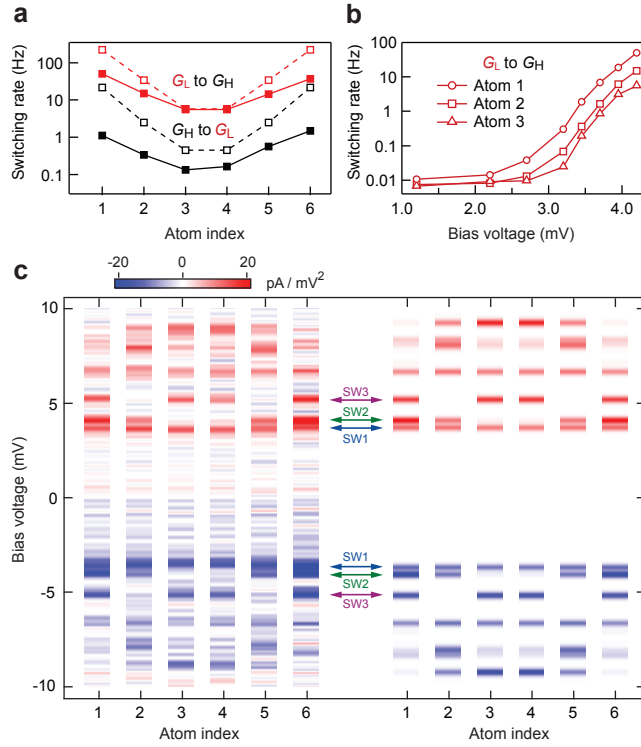


Figure 8. (a) Telegraph noise switching rates in both directions plotted as a function of position along the chain. Filled markers connected with solid line are the experimental data, open markers connected with dashed line are the theoretical simulations. For this measurement: sample bias voltage $V = 4.2$ mV, magnetic field $B = 200$ mT and temperature $T = 330$ mK. (b) Measured switching rates from the low conductance state G_L to the high conductance G_H as a function of the applied voltage, for the first three atoms of the chain. Magnetic field and temperature same as (a). (c) IETS spectra (d^2I/dV^2) as a function of position along the chain, at $B = 200$ mT and $T = 330$ mK. The left panel shows the experimental data; the right side the corresponding simulations. The three lowest energy excitations, that are confined spin waves, are identified. All panels reproduced from Ref. [22].

On a ferromagnetic Fe chain, the switching rates measured along the chain are not constant. The observed spatial dependence of the switching rates of a six-atom chain

is shown in figure 8a for a specific value of applied voltage. Not only is the switching fastest on the outer atoms (atoms 1 and 6), also atoms 2 and 5 have a rate that is significantly higher than the rate found on atoms 3 and 4. As such, explanations based on the fact that the outer atoms, unlike the inner atoms, have only one neighbour and are therefore easier to switch can be discarded. Also, a strong dependence on the applied voltage is observed (figure 8b): when the applied voltage is $V \sim 3.5$ mV, the switching rates rapidly increase for all the atoms in the chain.

To shed some light into this behaviour, IETS spectra were measured with a non polarized tip, as a function of atom position along the chain. Recorded spectra and corresponding simulations are shown in figure 8c. Instead of the usual dI/dV , here the color scale shows its derivative (d^2I/dV^2): the spin excitations appear as peaks (dips) for positive (negative) sample voltage, at the same energies of the steps in the corresponding differential conductance curves. Surprisingly, the first excitation occurs at the same energy along the chain and has the same intensity for all atoms. Apparently these are truly collective excitations of the chain and no difference is observed between atoms having one neighbour (atoms 1 and 6) and those having two. The second excited state, at an energy very close to the first, and the third have both a nodal modulation along the chain: they are less intense on the center atoms and on atoms 2 and 5 respectively. These three low energy states are identified as standing spin waves confined in the chain.

The dependence of the switching rate on the bias voltage can be explained by noting that the value at which the rates start to rise corresponds to the inelastic excitation threshold: the tip is driving the switching by excitations above the energy barrier. However, this first spin wave state SW1 is homogeneous along the chain, so it cannot explain the observed spatial dependence. But the second excited state SW2 is very close in energy, and with theoretical models based on Pauli master equations, it can be shown that there is a non negligible probability that, once the system is excited in SW1 by the tip, a chain of subsequent excitations occurs, temporarily occupying SW2 (that is responsible for the spatial modulation) and ending up on the other side of the barrier. So, to controllably revert the magnetization of a ferromagnet, the easiest way is by exciting it into a spin wave state with a node on the center, that can assist the switching [22, 111].

5.3. Back-action onto the tip

In most experiments involving spin-polarized STM, the tip is considered to be either permanently magnetized or, when polarization is achieved by picking up one or a few magnetic atoms, paramagnetic and thereby constantly oriented in the direction of an external magnetic field. Considering the low coordination of atoms at the apex of a tip, however, the assumption of static polarization is likely not very realistic. In this section we will show novel data on magnetic switching that can be used to extract information about the STM tip itself.

Not much it is known about the few atoms close to the tip apex that are actually

taking part in the tunnelling process. Whereas the bulk material of the tip is typically a hard metal (e.g. PtIr), in order to make it atomically sharp, it is regularly indented in the softer metal substrate. In our experiments the sample is a copper crystal, so we can imagine our tip to be copper coated. In order to polarize the tip, a single magnetic (e.g. Fe) atom is picked up to replace the apex Cu atom. This stage cannot be controlled very well: sometimes during manipulation Fe atoms are picked up but cannot be released afterwards. Therefore, the number of Fe atoms on the tip and how they are exactly positioned is unknown. Consequently, the manner in which the tip will respond to its environment, e.g. an external magnetic field or a stray field induced by the sample, is not predictable. Due to interactions acting back onto the tip, the observed switching behaviour of a bistable structure detected by the tip may be non-uniform along the structure. As demonstrated below, these variations can be used to extract information about the tip apex.

At the beginning of this section, we have introduced the antiferromagnetic Fe structures exhibiting bistable behaviour, measured in Ref. [19]. We have reproduced this experiment obtaining similar results concerning switching rates. However, in some cases we observed a spatial variation in the switching amplitude not reported before. In particular, we found two remarkable facts. First, the difference in conductance between the two Néel states (and consequently the tip height difference Δy) was more pronounced for the outer atoms of the chain than for all the others; two examples of those different amplitude telegraph noise switching traces are shown in figures 9a–b. Second, for the inner atoms of the chain, a subatomic periodicity was found: the largest switching amplitude was not measured on top of the atoms but slightly off either side of the atom. A measurement of Δy as a function of position along the chain is presented in figures 9d–e, for a chain with six Fe atoms. As can be seen by the density of experimental points, several data points at fixed distance within each other have been acquired per atom. This allows to see how the switching traces vary while the tip is moving across each atom of the chain. For reference, in figure 9c the topography, measured simultaneously with the switching data, is presented.

As discussed in section 3.3, in a spin-polarized STM measurement, the tunnel current can be expressed as the non polarized component times a term that depends on the product between tip and sample polarizations and the cosine of the angle β between the two magnetization directions (5). For the chain studied here, in the ground state the easy-axis anisotropy of the Fe atoms on Cu₂N aligns the spins along the direction in which the chain is built (defined as z -direction) [19]. At zero magnetic field this results in two degenerate ground states (the Néel states) with alternating spin orientations. By restricting our attention only to the two Néel states and magnetic fields applied along z , the angles between the spin polarization of the tip and the j -atom in the chain can only be $\beta_j = 0$ or $\beta_j = \pi$. So the spin polarized current of one Néel state becomes (P_j^S

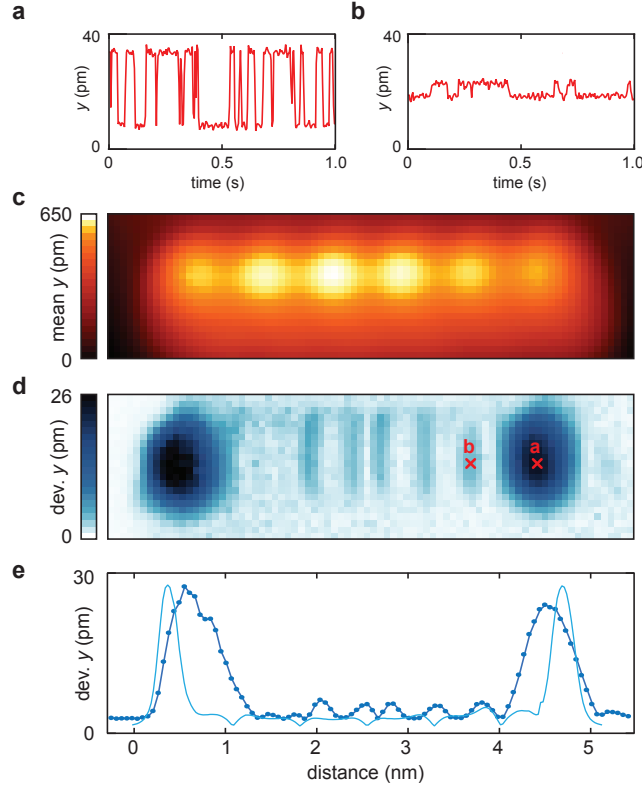


Figure 9. (a)-(b) Two examples of telegraph noise traces measured, respectively, for an outer and an inner atom of a chain composed of 6 Fe atoms antiferromagnetically coupled to each other. Exact locations where those traces were recorded is shown in (d). (c) Mean value of the measured tip height (i.e. topography) as a function of the spatial position. (d) Standard deviation of the height distribution along the chain, showing switching amplitudes as a function of position. (e) Line-cut of (d) along the center of the chain (marks connected with dark blue line), showing the variations in tip height along when the tip is moving from atom to atom. It is interesting to note the ratio of the peaks for outer and inner atoms and the structure in correspondence of the inner atoms. The (thinner) light blue line is the simulated curve, based on the model described in section 5.3.

is the polarization of the j -th atom of the chain):

$$I_{\text{SP}}(\mathbf{d}) \propto \sum_{j=1}^n I_0(\mathbf{d}) \left[1 + (-1)^j P^T P_j^S \right]. \quad (14)$$

The expression for the current of the other Néel state will be the same but with inverted atom polarizations (i.e. substitute $(-1)^j$ with $(-1)^{j+1}$ in (14)).

Here we present a model based on the notion that the magnetic atom located at the tip apex can pivot around the apex. The magnetic atom is represented as a pendulum subject to an harmonic potential, that is influenced both by the external magnetic field and the stray field induced by the magnetic structure on the surface. As a result, the chain switching behaviour detected by the tip will be non uniform along the structure. A similar model has been proposed by Hapala and coworkers [112] to

explain the high-resolution molecular imaging of molecules by means of IETS described in Ref. [113].

We assume that the atomic spins of the antiferromagnetic chain will generate a stray field, that can be modelled as the total magnetic field created by the magnetic dipole moments $\boldsymbol{\mu}_j$, positioned at each atom site \mathbf{r}_j . Each dipole will generate a magnetic field at position \mathbf{r} , $\mathbf{B}_j(\mathbf{r})$, that can be written as [114]:

$$\mathbf{B}_j(\mathbf{r}) = \frac{\mu_0}{4\pi |\mathbf{d}|^3} \left[3 \left(\boldsymbol{\mu}_j \cdot \hat{\mathbf{d}} \right) \hat{\mathbf{d}} - \boldsymbol{\mu}_j \right] + \frac{2\mu_0}{3} \boldsymbol{\mu}_j \delta^3(\mathbf{d}). \quad (15)$$

In the previous equation, μ_0 is the vacuum permeability, $\delta^3(\mathbf{d})$ is the three-dimensional Dirac delta function, $\mathbf{d} \equiv (\mathbf{r} - \mathbf{r}_j)$ is the relative distance between the position where the field is measured \mathbf{r} and the position \mathbf{r}_j of the magnetic moment $\boldsymbol{\mu}_j$ (where $\hat{\mathbf{d}}$ denotes the unit vector in the direction of \mathbf{d}). Since all the dipole moments of the chain are assumed to be oriented along the z -axis and the Fe atoms on Cu_2N have spin $S = 2$, we can write $\boldsymbol{\mu}_j = \pm(-1)^{j+1}2g\mu_B\hat{z}$, with the \pm sign identifying one of the two possible Néel states. The total stray field generated by the structure will then be the sum of all the dipole moments contributions:

$$\mathbf{B}(\mathbf{r}) = \sum_{j=1}^n \mathbf{B}_j(\mathbf{r}). \quad (16)$$

The calculated stray field (16) felt by the tip at a typical tip-sample distance of 3 Å is a few mT, much smaller than typical values of external magnetic field applied during the experiment. However, a non-uniform field, like the one generated by the Fe chain, will also exert a force on any magnetic dipole, like the dipole moment $\boldsymbol{\mu}_{\text{apex}}$ associated to the spin of the apex atom of the spin polarized tip. The force is given by:

$$\mathbf{F}_{\text{Dipole}} = \nabla \left(\boldsymbol{\mu}_{\text{apex}} \cdot \mathbf{B} \right), \quad (17)$$

where $\nabla \equiv [(\partial/\partial x)\hat{x} + (\partial/\partial y)\hat{y} + (\partial/\partial z)\hat{z}]$ is the gradient operator and $\boldsymbol{\mu}_{\text{apex}} = -2g\mu_B\hat{z}$ if the external field is oriented along the negative z -direction.

When the chain switches from one Néel state to the other, the stray magnetic field (16) changes sign, and this leads to $\mathbf{F}_{\text{Dipole}} \rightarrow -\mathbf{F}_{\text{Dipole}}$. The external magnetic field, on the other hand, is uniform and thereby does not exert any force on the tip apex atom. As such, the potential energy of the tip due to the magnetic field is given by (with B_z the z -component of the stray field):

$$U_{\text{Dipole}} = -\mu_{\text{apex}} B_z. \quad (18)$$

The displacement of the magnetic apex atom due to the stray field generated by the structure may affect the switching signal as follows. Let's assume the apex atom is bound to a single non magnetic atom of the tip (see figure 10a), that we call the pivot atom. We treat those two atoms as hard spheres, with a fixed distance $d = 1$ Å between their respective centres. The apex atom is allowed to rotate in the two directions identified with the angles ϕ_a and θ_a . If we treat this system as a simple harmonic oscillator, the

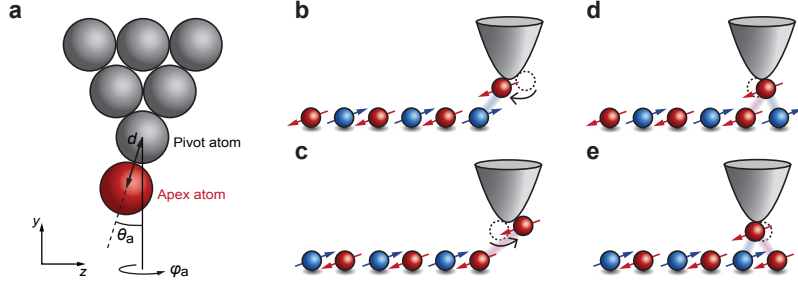


Figure 10. (a) Schematic of the last few atoms of the tip according to the pendulum-tip model. (b)-(e) Illustration of the motion of the tip apex in response of the stray magnetic field generated by the structure in both Néel states. Near the edge of the chain (b,c), the motion will be much more dramatic than over the center of the chain (d,e), where the apex atom feels conflicting influences from neighbouring atoms in the structure.

apex atom will have, at position θ_a , a potential energy given by $\frac{1}{2}K\theta_a^2$. Furthermore, we restrict the motion of the atom to $0 \leq \theta_a \leq \pi/4$.

The total potential energy felt by the apex atom will be a function of the position of the pivot-atom above the chain \mathbf{r}_T and the spherical coordinates of the apex-atom with respect to the pivot (ϕ_a, θ_a) :

$$V(\mathbf{r}_T, \theta_a, \phi_a) = \frac{1}{2}K\theta_a^2 - \mu_{\text{apex}}B_z(y_T, z_T, \theta_a, \phi_a). \quad (19)$$

The equilibrium position of the apex atom can be determined by numerical minimization of (19) with respect to the spherical coordinates (ϕ_a, θ_a) for a fixed pivot position \mathbf{r}_T above the chain. This leads to an equilibrium position $(\phi_{\text{eq}}, \theta_{\text{eq}})$ from which the apex position \mathbf{r}_{apex} above the chain can be determined. Once this position is known, we can calculate the corresponding polarized tunnel current for the two Néel states by using (14), and therefore their difference. Performing this algorithm for a range of tip positions along the chain z_T and different tip height y_T , we can simulate the switching data as shown in figure 9e.

In this model the work function φ of the tunnel barrier was used as a fitting parameter. This quantity enters in the non-polarized current (4) via the following relation:

$$\varphi = \frac{\hbar^2 \kappa^2}{2m}, \quad (20)$$

with κ being the decay rate of the tunnel current with increasing distance, m the electron mass and \hbar the reduced Planck constant. From the fits, we have obtained a work function of $\varphi = 3.8$ eV, very close to the typical value of a tunnel junction $\varphi = 4.2$ eV.

The simulated switching curve show qualitative agreement with the measured data, e.g. the large relative peak height of the outer atoms compared to the inner atoms of the chain and the appearance of a subatomic double periodicity on the inner atoms.

Figures 10b–e show an interpretation of the motion of the apex atom when it is subject to the force due to the chain stray field $\mathbf{F}_{\text{Dipole}}$ in the proposed model. The difference in peak height between inner and outer atoms comes out naturally when assuming a spin polarized current tunnelling not only into the atom straight underneath the tip but also diagonally into the two neighbouring atoms, with opposite magnetization direction. The effect of the signal coming from those two atoms cancels out part of the spin polarized current, and this reduces the apparent tip height variation. This effect will be smaller when tunnelling into the outer atoms that have only one neighbour. No pivoting atom is needed to explain this observation. The double periodicity found on the inner atoms of the chain, however, cannot be reproduced without introducing the stray field induced by the structure on the pivot atom.

In this way we have shown how, starting from switching data measured on a bistable chain, we can gain information on the functionalized spin-polarized tip, that is otherwise considered an unknown parameter in most of STM experiments. We note that the effect described in this chapter may be related to what was very recently shown in Ref. [110], in which the magnetic structure interacts with the STM tip via exchange interaction.

6. Conclusions and outlook

In this paper we have reviewed the state of the art of the atomic scale magnetism studied by means of a scanning tunneling microscope. Low dimensional magnetism is a topic that has attracted a lot of theoretical interest, starting from the early works of Ising [24], Bethe [115] and Heisenberg [116] at the end of the 1920s. Only very recently, it has been possible to experimentally build magnetic lattices, using vertical atom manipulation, and probe them locally. This is a very promising avenue for realizing quantum mechanical systems and study their transitions to the classical limit.

After reviewing the principal experimental techniques needed for this fascinating study, in this work we have summarized the principal aspects of the physics of single spins. When an atom is embedded in a surface, it can develop a magnetocrystalline anisotropy, that is a result of the interplay between the spin-orbit coupling and the crystal field splitting induced by the broken symmetries of the surface. A magnetic impurity on a surface can also be Kondo-screened by the substrate electrons and it can react to an externally applied magnetic field, due to the Zeeman effect. Finally, two magnetic atoms can interact with each other, and the strength and sign of their interaction will depend on their relative distance. Here we have shown how all those physical properties can not only be probed but also tuned by adjusting the exact position of an atom (or of few atoms) on a substrate.

All those effects can give rise to magnetic bistability. Very recently a few examples of systems composed only of a few atoms have been proven to be bistable, opening the way to new approaches towards the realization of nanoscale magnetic storage devices. Next to showing some techniques to actually detect this bistability, even in cases for which conventional measurements are not sufficient, we have given an insight on the role

played by standing spin waves in order to revert the magnetization of a ferromagnet composed of only few atoms. Finally, we have shown how data collected on a bistable structure could be used to extract useful information on the apex of an STM tip, the part that is actually involved in the tunnelling process.

Now that structures with ferromagnetic and antiferromagnetic interactions can be atomically engineered, the way is paved for experiments in which we can look at the evolution of spinons and magnons in one- and two-dimensional lattices. Unlike other techniques used to study quantum magnetism, e.g. ultracold atoms, the field of atomic engineering enables to make customized modification to the lattice, like local substitutional doping, defects injection or magnetic frustration. We foresee that this approach is reaching a state of maturity where we expect a synergy to be created between experimental atomic surface science and theoretical quantum magnetism.

References

- [1] Eigler D M and Schweizer E K 1990 *Nature* **344** 524–526 ISSN 0028-0836 URL <http://www.nature.com/doifinder/10.1038/344524a0>
- [2] Heinrich A J, Gupta J A, Lutz C P and Eigler D M 2004 *Science* **306** 466 ISSN 1095-9203 URL <http://www.sciencemag.org/content/306/5695/466.short>
- [3] Meier F, Zhou L, Wiebe J and Wiesendanger R 2008 *Science (New York, N.Y.)* **320** 82–86 ISSN 1095-9203 URL <http://www.sciencemag.org/content/320/5872/82.short>
- [4] Hirjibehedin C F, Lin C Y, Otte A F, Ternes M, Lutz C P, Jones B A and Heinrich A J 2007 *Science (New York, N.Y.)* **317** 1199–1203 ISSN 1095-9203 URL <http://www.sciencemag.org/content/317/5842/1199.short>
- [5] Bryant B, Spinelli A, Wagenaar J J T, Gerrits M and Otte A F 2013 *Physical Review Letters* **111** 127203 ISSN 0031-9007 URL <http://link.aps.org/doi/10.1103/PhysRevLett.111.127203>
- [6] Khajetoorians A A, Schlenk T, Schweffinghaus B, dos Santos Dias M, Steinbrecher M, Bouhassoune M, Lounis S, Wiebe J and Wiesendanger R 2013 *Physical Review Letters* **111** 157204 ISSN 0031-9007 URL <http://link.aps.org/doi/10.1103/PhysRevLett.111.157204>
- [7] Oberg J C, Calvo M R, Delgado F, Moro-Lagares M, Serrate D, Jacob D, Fernández-Rossier J and Hirjibehedin C F 2014 *Nature nanotechnology* **9** 64–8 ISSN 1748-3395 URL <http://www.ncbi.nlm.nih.gov/pubmed/24317285>
- [8] Madhavan V, Chen W, Jamneala T, Crommie M F and Wingreen N S 1998 *Science* **280** 567–569 ISSN 00368075 URL <http://www.sciencemag.org/content/280/5363/567.short>
- [9] Wahl P, Diekhöner L, Schneider M, Vitali L, Wittich G and Kern K 2004 *Physical Review Letters* **93** 176603 ISSN 0031-9007 URL <http://link.aps.org/doi/10.1103/PhysRevLett.93.176603>
- [10] Néel N, Kröger J, Limot L, Palotas K, Hofer W and Berndt R 2007 *Physical Review Letters* **98** 16801 ISSN 0031-9007 URL <http://link.aps.org/doi/10.1103/PhysRevLett.98.016801>
- [11] Otte A F, Ternes M, von Bergmann K, Loth S, Brune H, Lutz C P, Hirjibehedin C F and Heinrich A J 2008 *Nature Physics* **4** 847–850 ISSN 1745-2473 URL <http://www.nature.com/doifinder/10.1038/nphys1072>
- [12] Wahl P, Simon P, Diekhöner L, Stepanyuk V S, Bruno P, Schneider M A and Kern K 2007 *Physical Review Letters* **98** 056601 ISSN 0031-9007 URL <http://link.aps.org/doi/10.1103/PhysRevLett.98.056601>
- [13] Otte A F, Ternes M, Loth S, Lutz C P, Hirjibehedin C F and Heinrich A J 2009 *Physical Review Letters* **103** 107203 ISSN 0031-9007 URL <http://link.aps.org/doi/10.1103/PhysRevLett.103.107203>

- [14] Zhou L, Wiebe J, Lounis S, Vedmedenko E, Meier F, Blügel S, Dederichs P H and Wiesendanger R 2010 *Nature Physics* **6** 187–191 ISSN 1745-2473 URL <http://www.nature.com/doifinder/10.1038/nphys1514>
- [15] Hirjibehedin C F, Lutz C P and Heinrich A J 2006 *Science (New York, N.Y.)* **312** 1021–4 ISSN 1095-9203 URL <http://www.sciencemag.org/content/312/5776/1021.short>
- [16] Néel N, Berndt R, Kröger J, Wehling T O, Lichtenstein A I and Katsnelson M I 2011 *Physical Review Letters* **107** 106804 ISSN 0031-9007 URL <http://link.aps.org/doi/10.1103/PhysRevLett.107.106804>
- [17] Khajetoorians A A, Wiebe J, Chilian B, Lounis S, Blügel S and Wiesendanger R 2012 *Nature Physics* **8** 497–503 ISSN 1745-2473 URL <http://www.nature.com/doifinder/10.1038/nphys2299>
- [18] Khajetoorians A A, Wiebe J, Chilian B and Wiesendanger R 2011 *Science* **332** 1062 URL <http://www.sciencemag.org/content/332/6033/1062.short>
- [19] Loth S, Baumann S, Lutz C P, Eigler D M and Heinrich A J 2012 *Science (New York, N.Y.)* **335** 196–199 ISSN 1095-9203 URL <http://www.ncbi.nlm.nih.gov/pubmed/22246771>
- [20] Khajetoorians A A, Baxevanis B, Hübner C, Schlenk T, Krause S, Wehling T O, Lounis S, Lichtenstein A, Pfannkuche D, Wiebe J and Wiesendanger R 2013 *Science* **339** 55–9 ISSN 1095-9203 URL <http://www.sciencemag.org/content/339/6115/55.short>
- [21] Miyamachi T, Schuh T, Märkl T, Bresch C, Balashov T, Stöhr A, Karlewski C, André S, Marthaler M, Hoffmann M, Geilhufe M, Ostanin S, Hergert W, Mertig I, Schön G, Ernst A and Wulfhekel W 2013 *Nature* **503** 242–6 ISSN 1476-4687 URL <http://www.nature.com/doifinder/10.1038/nature12759>
- [22] Spinelli A, Bryant B, Delgado F, Fernández-Rossier J and Otte A F 2014 *Nature materials* **13** 782–785 ISSN 1476-1122 URL <http://www.nature.com/nmat/journal/v13/n8/full/nmat4018.html>
- [23] Mourigal M, Enderle M, Klöpperpieper A, Caux J S, Stunault A and Rønnow H M 2013 *Nature Physics* **9** 435–441 ISSN 1745-2473 URL <http://www.nature.com/doifinder/10.1038/nphys2652>
- [24] Ising E 1925 *Zeitschrift für Physik* **31** 253–258
- [25] Brush S G 1967 *Reviews of Modern Physics* **39** 883
- [26] Anderson P W 1973 *Materials Research Bulletin* **8** 153–160 URL <http://www.sciencedirect.com/science/article/pii/0025540873901670>
- [27] Ramirez A P 2008 *Nature* **4** 442
- [28] Balents L 2010 *Nature* **464** 199–208 ISSN 1476-4687 URL <http://www.nature.com/nature/journal/vaop/ncurrent/full/nature08917.html>
- [29] Mila F F 2000 *European Journal of Physics* **21** 499–510 ISSN 0143-0807 URL <http://iopscience.iop.org/0143-0807/21/6/302>
- [30] Affleck I 1999 *Journal of Physics: Condensed Matter* **1** 3047–3072
- [31] Mermin N D and Wagner H 1966 *Physical Review Letters* **17** 1133–1136
- [32] Bose I 2006 *Current Science* **37** 62–70 ISSN 0931-7597
- [33] Lecheminant P 2003 60 (*Preprint 0306520*) URL <http://arxiv.org/abs/cond-mat/0306520>
- [34] Lacroix C, Mendels P and Mila F (eds) 2011 *Introduction to Frustrated Magnetism (Springer Series in Solid-State Sciences vol 164)* (Berlin, Heidelberg: Springer Berlin Heidelberg) ISBN 978-3-642-10588-3 URL <http://link.springer.com/10.1007/978-3-642-10589-0>
- [35] Bloch I, Dalibard J and Nascimbène S 2012 *Nature Physics* **8** 267–276 ISSN 1745-2473 URL <http://www.nature.com/doifinder/10.1038/nphys2259>
- [36] Binnig G, Rohrer H, Gerber C and Weibel E 1982 *Applied Physics Letters* **40** 178 ISSN 00036951 URL <http://scitation.aip.org/content/aip/journal/apl/40/2/10.1063/1.92999>
- [37] Binnig G, Rohrer H, Gerber C and Weibel E 1982 *Physical review letters* **49** 57–61 URL <http://journals.aps.org/prl/abstract/10.1103/PhysRevLett.49.57>
- [38] Crommie M F, Lutz C P and Eigler D M 1993 *Science (New York, N.Y.)* **262** 218–220 ISSN

0036-8075

- [39] Heinrich A J, Lutz C P, Gupta J A and Eigler D M 2002 *Science (New York, N.Y.)* **298** 1381–1387 ISSN 1095-9203 URL <http://www.sciencemag.org/content/298/5597/1381.short>
- [40] Gomes K K, Mar W, Ko W, Guinea F and Manoharan H C 2012 *Nature* **483** 306–310 ISSN 1476-4687 URL <http://www.ncbi.nlm.nih.gov/pubmed/22422264>
- [41] Leibsle F M, Flipse C F J and Robinson A W 1993 *Physical Review B* **47** 15865 URL http://prb.aps.org/abstract/PRB/v47/i23/p15865_1
- [42] Eigler D M, Lutz C P and Rudge W E 1991 *Nature* **352** 600 URL <http://www.nature.com/nature/journal/v352/n6336/abs/352600a0.html>
- [43] Hla S w 2005 1–12 (*Preprint 0506038*) URL <http://arxiv.org/abs/cond-mat/0506038>
- [44] Ghosh C, Kara A and Rahman T S 2002 *Surface Science* **502-503** 519–526 ISSN 00396028 URL <http://linkinghub.elsevier.com/retrieve/pii/S0039602801020015>
- [45] Jaklevic R C and Lambe J 1966 *Physical Review Letters* **17** 1139–1140 ISSN 0031-9007 URL <http://link.aps.org/doi/10.1103/PhysRevLett.17.1139>
- [46] Stipe B C 1998 *Science* **280** 1732–1735 ISSN 00368075 URL <http://www.sciencemag.org/content/280/5370/1732.short>
- [47] Fernández-Rossier J 2009 *Physical Review Letters* **102** 256802 ISSN 0031-9007 URL <http://link.aps.org/doi/10.1103/PhysRevLett.102.256802>
- [48] Persson M 2009 *Physical Review Letters* **103** 50801 ISSN 0031-9007 URL <http://link.aps.org/doi/10.1103/PhysRevLett.103.050801>
- [49] Fransson J 2009 *Nano letters* **9** 2414–2417 ISSN 1530-6992 URL <http://www.ncbi.nlm.nih.gov/pubmed/19507889>
- [50] Lorente N and Gauryacq J P 2009 *Physical Review Letters* **103** 176601 ISSN 0031-9007 URL <http://link.aps.org/doi/10.1103/PhysRevLett.103.176601>
- [51] Loth S, von Bergmann K, Ternes M, Otte A F, Lutz C P and Heinrich A J 2010 *Nature Physics* **6** 340–344 ISSN 1745-2473 URL <http://www.nature.com/doi/10.1038/nphys1616>
- [52] Nazarov Y V and Blanter Y M 2009 *Quantum Transport: Introduction to Nanoscience* (Cambridge University Press) ISBN 9781139478175 URL <http://books.google.nl/books?id=bjmXJOFmqZIC>
- [53] Delgado F and Fernández-Rossier J 2011 *Physical Review B* **84** 45439 ISSN 1098-0121 URL <http://link.aps.org/doi/10.1103/PhysRevB.84.045439>
- [54] Delgado F and Fernández-Rossier J 2010 *Physical Review B* **82** 134414 ISSN 1098-0121 URL <http://link.aps.org/doi/10.1103/PhysRevB.82.134414>
- [55] Lambe J and Jaklevic R 1968 *Physical Review* **165** 165 URL <http://journals.aps.org/pr/abstract/10.1103/PhysRev.165.821>
- [56] Kogan A, Amasha S, Goldhaber-Gordon D, Granger G, Kastner M and Shtrikman H 2004 *Physical Review Letters* **93** 166602 ISSN 0031-9007 URL <http://link.aps.org/doi/10.1103/PhysRevLett.93.166602>
- [57] Otte A F 2008 *Magnetism of a Single Atom. Leiden University (2008)* Ph.D. thesis Leiden University URL <http://hdl.handle.net/1887/12660>
- [58] Zhang Y h, Kahle S, Herden T, Stroh C, Schlickum U, Ternes M, Wahl P, Kern K and Mayor M 2013 *Nature communications* **4** 2110 ISSN 2041-1723 URL <http://www.pubmedcentral.nih.gov/articlerender.fcgi?artid=3730050&tool=pmcentrez&rendertype=abstract>
- [59] Spinelli A, Gerrits M, Toskovic R, Bryant B, Ternes M and Otte A F 2014 1–5 (*Preprint 1411.4415*) URL <http://arxiv.org/abs/1411.4415>
- [60] Chen X, Fu Y S, Ji S H, Zhang T, Cheng P, Ma X C, Zou X L, Duan W H, Jia J F and Xue Q K 2008 *Physical Review Letters* **101** 197208 ISSN 0031-9007 URL <http://prl.aps.org/abstract/PRL/v101/i19/e197208>
- [61] Tsukahara N, Noto K i, Ohara M, Shiraki S, Takagi N, Shin S, Kawai M, Takata Y, Miyawaki J, Taguchi M and Chainani A 2009 *Physical Review Letters* **102** 167203 ISSN 0031-9007 URL <http://link.aps.org/doi/10.1103/PhysRevLett.102.167203>

- [62] Khajetoorians A A, Chilian B, Wiebe J, Schuwalow S, Lechermann F and Wiesendanger R 2010 *Nature* **467** 1084–1087 ISSN 1476-4687 URL <http://www.nature.com/nature/journal/v467/n7319/abs/nature09519.html>
- [63] Averin D and Nazarov Y 1990 *Physical Review Letters* **65** 2446–2449 ISSN 0031-9007 URL <http://link.aps.org/doi/10.1103/PhysRevLett.65.2446>
- [64] De Franceschi S, Sasaki S, Elzerman J, van der Wiel W, Tarucha S and Kouwenhoven L P 2001 *Physical Review Letters* **86** 878–881 ISSN 0031-9007 URL <http://link.aps.org/doi/10.1103/PhysRevLett.86.878>
- [65] Zumbühl D, Marcus C, Hanson M and Gossard A 2004 *Physical Review Letters* **93** 256801 ISSN 0031-9007 URL <http://link.aps.org/doi/10.1103/PhysRevLett.93.256801>
- [66] Schleser R, Ihn T, Ruh E, Ensslin K, Tews M, Pfannkuche D, Driscoll D and Gossard A 2005 *Physical Review Letters* **94** 206805 ISSN 0031-9007 URL <http://link.aps.org/doi/10.1103/PhysRevLett.94.206805>
- [67] Pierce D T 1988 *Physica Scripta* **38** 291–296 URL <http://iopscience.iop.org/1402-4896/38/2/035>
- [68] Wiesendanger R, Guntherodt H J, Guntherodt G, Gambino R J and Ruf R 1990 *Physical Review Letters* **65** 247–251
- [69] Wiesendanger R, Shvets I V, Burgler D, Tarrach G, Gujnterodt H J, Coey J M D and Graser 1992 *Science* **255** 583
- [70] Heinze S, Bode M, Kubetzka A, Pietzsch O, Nie X, Blügel S and Wiesendanger R 2000 *Science* **288** 1805–1808 ISSN 00368075 URL <http://www.sciencemag.org/cgi/doi/10.1126/science.288.5472.1805>
- [71] Bode M, Heide M and Bergmann K V 2007 *Nature* **447** 190–193 ISSN 1476-4687 URL <http://www.nature.com/nature/journal/v447/n7141/abs/nature05802.html>
- [72] Gao C L, Wulffhel W and Kirschner J 2008 *Physical review letters* **101** 267205 ISSN 0031-9007 URL <http://link.aps.org/doi/10.1103/PhysRevLett.101.267205>
- [73] Bode M 2003 *Reports on Progress in Physics* **66** 523–582 URL <http://iopscience.iop.org/0034-4885/66/4/203>
- [74] Wiesendanger R 2009 *Reviews of Modern Physics* **81** 1495–1550 ISSN 0034-6861 URL <http://link.aps.org/doi/10.1103/RevModPhys.81.1495>
- [75] Sonntag A, Hermenau J, Schlenhoff A, Friedlein J, Krause S and Wiesendanger R 2014 *Physical Review Letters* **112** 017204 ISSN 0031-9007 URL <http://link.aps.org/doi/10.1103/PhysRevLett.112.017204>
- [76] Yamada T K, Bischoff M M J, Mizoguchi T and van Kempen H 2003 *Applied Physics Letters* **82** 1437 ISSN 00036951 URL <http://scitation.aip.org/content/aip/journal/apl/82/9/10.1063/1.1556958>
- [77] Berbil-Bautista L, Krause S, Bode M and Wiesendanger R 2007 *Physical Review B* **76** 064411 ISSN 1098-0121 URL <http://link.aps.org/doi/10.1103/PhysRevB.76.064411>
- [78] Tersoff J and Hamann D 1983 *Physical review letters* **50** 1998–2001 URL <http://journals.aps.org/prl/abstract/10.1103/PhysRevLett.50.1998>
- [79] Tersoff J and Hamann D 1985 *Physical Review B* **31** 805 URL http://link.springer.com/chapter/10.1007/978-94-011-1812-5_5
- [80] Bardeen J 1961 *Physical Review Letters* **6** 57 URL <http://journals.aps.org/prl/abstract/10.1103/PhysRevLett.6.57>
- [81] Gatteschi D, Sessoli R and Villain J 2006 *Molecular nanomagnets* (Oxford: Oxford University Press) ISBN 978-0-19-856753-0
- [82] Kramers H A 1930 *Proc. Amst. Acad.* **33** 959
- [83] Pryce M H L 1950 *Proc. Phys. Soc. London Sect. A* **63** 25 ISSN 0370-1298 URL <http://iopscience.iop.org/0370-1298/63/1/304>
- [84] Dai D, Xiang H and Whangbo M H 2008 *J Comput Chem* **29** 2187 ISSN 1096-987X URL <http://www.ncbi.nlm.nih.gov/pubmed/18484639>

- [85] Griffiths D J 2005 *Introduction to Quantum Mechanics* Pearson international edition (Pearson Prentice Hall) ISBN 9780131118928 URL http://books.google.nl/books?id=9sqIaRGx_EoC
- [86] Koch E 2012 Exchange Mechanism *Modeling and Simulation, Forschungszentrum Julich* vol 2 chap 7 ISBN 9783893367962
- [87] Ruderman M A and Kittel C 1954 *Physical Review* **96** 99 URL <http://journals.aps.org/pr/abstract/10.1103/PhysRev.96.99>
- [88] Kasuya T 1956 *Progress of theoretical physics* **16** 45–57
- [89] Yosida K 1957 *Physical Review* **106** 893 URL <http://journals.aps.org/pr/abstract/10.1103/PhysRev.106.893>
- [90] Anderson P W 1961 *Physical Review* **124** 41–53 ISSN 0031-899X URL <http://link.aps.org/doi/10.1103/PhysRev.124.41>
- [91] Hewson A C 1997 *The Kondo Problem to Heavy Fermions* Cambridge Studies in Magnetism (Cambridge University Press) ISBN 9780521599474 URL <http://books.google.nl/books?id=fPzgHneNFDAC>
- [92] Kondo J 1964 *Progress of theoretical physics* **32** 37–49 URL <http://ptp.oxfordjournals.org/content/32/1/37.short>
- [93] Haas W J D and den Berg G J V 1936 *Physica* 440–449 URL <http://www.sciencedirect.com/science/article/pii/S0031891436800093>
- [94] Cronenwett S M 1998 *Science* **281** 540–544 URL <http://www.sciencemag.org/content/281/5376/540.short>
- [95] Goldhaber-Gordon D, Göres J, Kastner M, Shtrikman H, Mahalu D and Meirav U 1998 *Physical Review Letters* **81** 5225–5228 ISSN 0031-9007 URL <http://link.aps.org/doi/10.1103/PhysRevLett.81.5225>
- [96] Nygard J, Cobden D H and Lindelof P E 2000 *Nature* **408** 342–346 ISSN 0028-0836 URL <http://www.nature.com/nature/journal/v408/n6810/abs/408342a0.html>
- [97] Li J, Schneider W D, Berndt R and Delley B 1998 *Physical Review Letters* **80** 2893–2896 ISSN 0031-9007 URL http://prl.aps.org/abstract/PRL/v80/i13/p2893_1
- [98] Knorr N, Schneider M A, Diekhöner L, Wahl P and Kern K 2002 *Physical Review Letters* **88** 096804 ISSN 0031-9007 URL <http://link.aps.org/doi/10.1103/PhysRevLett.88.096804>
- [99] Madhavan V, Chen W, Jamneala T, Crommie M F and Wingreen N S 2001 *Physical Review B* **64** 165412 ISSN 0163-1829 URL <http://link.aps.org/doi/10.1103/PhysRevB.64.165412>
- [100] Nagaoka K, Jamneala T, Grobis M and Crommie M 2002 *Physical Review Letters* **88** 77205 ISSN 0031-9007 URL <http://link.aps.org/doi/10.1103/PhysRevLett.88.077205>
- [101] Jamneala T, Madhavan V, Chen W and Crommie M F 2000 *Physical Review B* **61** 9990–9993 ISSN 0163-1829 URL http://prb.aps.org/abstract/PRB/v61/i15/p9990_1
- [102] Skomski R 2003 *Journal of physics : Condensed matter* **15** R841 URL http://iopscience.iop.org/0953-8984/15/20/202/pdf/0953-8984_15_20_202.pdf
- [103] Chudnovskiy A, Hübner C, Baxevanis B and Pfannkuche D 2014 *physica status solidi B* **251** 1764–1776 ISSN 03701972 URL <http://doi.wiley.com/10.1002/pssb.201350225>
- [104] Gatteschi D and Sessoli R 2003 *Angewandte Chemie (International ed. in English)* **42** 268–297 ISSN 1433-7851 URL <http://www.ncbi.nlm.nih.gov/pubmed/12548682>
- [105] Leuenberger M N and Loss D 2001 *Nature* **410** 789–793
- [106] Krause S, Herzog G, Stapelfeldt T, Berbil-Bautista L, Bode M, Vedmedenko E and Wiesendanger R 2009 *Physical Review Letters* **103** 127202 ISSN 0031-9007 URL <http://link.aps.org/doi/10.1103/PhysRevLett.103.127202>
- [107] Herzog G, Krause S and Wiesendanger R 2010 *Applied Physics Letters* **96** 102505 ISSN 00036951 URL <http://scitation.aip.org/content/aip/journal/apl/96/10/10.1063/1.3354023>
- [108] Gambardella P, Dallmeyer A, Maiti K, Malagoli M C, Eberhardt W, Kern K and Carbone C 2002 *Nature* **416** 301–304 ISSN 0028-0836 URL <http://www.nature.com/nature/journal/v416/n6878/abs/416301a.html>
- [109] Loth S, Etzkorn M, Lutz C P, Eigler D M and Heinrich A J 2010 *Science (New York,*

- N.Y.*) **329** 1628–1630 ISSN 1095-9203 URL <http://www.sciencemag.org/content/329/5999/1628.short>
- [110] Yan S, Choi D J, Burgess J a J, Rolf-Pissarczyk S and Loth S 2014 *Nature nanotechnology* 1–6 ISSN 1748-3395 URL <http://www.ncbi.nlm.nih.gov/pubmed/25502311>
 - [111] Rohart S and Rodary G 2014 *Nature materials* **13** 770–1 ISSN 1476-1122 URL <http://www.nature.com/nmat/journal/v13/n8/full/nmat4038.html>
 - [112] Hapala P, Temirov R, Tautz F S and Jelínek P 2014 *Physical Review Letters* **113** 226101 ISSN 0031-9007 URL <http://link.aps.org/doi/10.1103/PhysRevLett.113.226101>
 - [113] Chiang C l, Xu C, Han Z and Ho W 2014 *Science (New York, N.Y.)* **344** 885–8 ISSN 1095-9203 URL <http://www.ncbi.nlm.nih.gov/pubmed/24855265>
 - [114] Griffiths D J and College R 1999 *Introduction to electrodynamics* (Prentice Hall) URL <http://www.ulb.tu-darmstadt.de/tocs/188898514.pdf>
 - [115] Bethe H 1931 *Zeitschrift fur Physik* **71** 205
 - [116] Heisenberg W 1928 *Zeitschrift fur Physik* **49** 205